

# Quantized Repetitions of the Cuprate Pseudogap Line

Vincent Sacksteder IV\*

*Department of Physics, Royal Holloway University of London,  
Egham Hill, Egham, TW20 0EX, United Kingdom*

The cuprate superconductors display several characteristic temperatures which decrease as the material composition is doped, tracing lines across the temperature-doping phase diagram. Foremost among these is the pseudogap transition. At a higher temperature a peak is seen in the magnetic susceptibility, and changes in symmetry and in transport are seen at other characteristic temperatures. We report a meta-analysis of all measurements of characteristic temperatures well above  $T_c$  in strontium doped lanthanum cuprate (LSCO) and oxygen doped YBCO. The experimental corpus shows that the pseudogap line is one of a family of four straight lines which stretches across the phase diagram from low to high doping, and from  $T_c$  up to 700 K. These lines all originate from a single point near the overdoped limit of the superconducting phase and increase as doping is reduced. The slope of the pseudogap lines is quantized, with the second, third, and fourth lines having slopes that are respectively  $1/2$ ,  $1/3$ , and  $1/4$  of the slope of the highest line. This pattern suggests that the cuprates host a single mother phase controlled by a 2-D sheet density which is largest at zero doping and which decreases linearly with hole density, and that the pseudogap lines, charge density wave order, and superconductivity are all subsidiary effects supported by the mother phase.

PACS numbers: 74.72.Gh,74.72.Kf,74.25.Dw

The cuprate high  $T_c$  superconductors are built from copper oxide planes, and when these planes are doped with holes superconductivity occurs. Temperatures above the superconducting critical temperature  $T_c$  make the cuprates effectively two dimensional by disrupting the weak interplane coupling. Nonetheless the cuprates exhibit a wide variety of mysterious features at temperatures far exceeding  $T_c$ . One of the first to be noticed is a broad peak in the magnetic susceptibility at a temperature  $T_{max}$ , which is accompanied by qualitative changes in electrical and thermal transport.<sup>38,99</sup> At low dopings  $T_{max}$  reaches temperatures as high as 700 K, and it decreases linearly as the parent compound is doped with holes. Focus has since shifted toward a pseudogap temperature  $T^*$  which is substantially smaller than  $T_{max}$  and again decreases linearly with hole doping.  $T^*$  marks a depletion in the density of states, and has been measured by many experimental techniques including angularly resolved photoemission spectroscopy (ARPES).<sup>68,87</sup> Over the years a perplexing cornucopia of other doping-dependent signals have been identified, including a lower pseudogap temperature  $T_\nu$ , charge density waves, nematic order, and a linear resistance extending to very high temperatures marking the "strange metal" regime.<sup>24,43</sup>

In this paper we identify an unexpected regularity in the cuprate phase diagram: four of the experimentally measured doping-dependent temperatures, including  $T_{max}$ , the pseudogap temperature  $T^*$ , and the lower pseudogap line  $T_\nu$ , belong to a family which radiates from a common intersection and has slopes determined by a quantization rule. Our results are based on a comprehensive and exhaustive survey of research papers which measure temperature dependence and report numerical values of characteristic temperatures well above  $T_c$ . We

report only characteristic temperatures at which clearly identifiable signals occur, for example peaks or kinks in the temperature dependence, or extinction of a diffraction peak at a particular temperature. In particular, the reported temperatures have been realized experimentally, rather than being derived by extrapolation from lower temperatures.

In order to remove any confusion about material-specific aspects of the phase diagram, we have separated data obtained from different compounds and doping techniques. We first report in Section I the characteristic temperatures of strontium-doped  $\text{La}_{2-x}\text{Sr}_x\text{CuO}_4$  (LSCO). Separately, in Section II we report the characteristic temperatures of oxygen-doped  $\text{YBa}_2\text{Cu}_3\text{O}_{6+\delta}$  (YBCO). These two compounds and doping strategies, plus a third compound  $\text{Bi}_2\text{Sr}_2\text{Ca}_{n-1}\text{Cu}_n\text{O}_{2n+4+\delta}$  (BSCCO), have been used for the large majority of data on characteristic temperatures of cuprates well above  $T_c$ ; our restriction to LSCO and YBCO is not terribly selective. In the following sections we compare the LSCO and YBCO data and draw conclusions about which aspects of the high  $T_c$  phase diagram are universal and which are material specific.

In gathering data we have followed standard practice among reviews of the high  $T_c$  phase diagram and the pseudogap by focusing on those experimental signals which are understood to reflect the carriers that mediate superconductivity, and omitting the extensive experimental literature that focuses on ionic behavior. Along these lines we omit thermal history dependence and hysteresis, oxygen movement and ordering, and mechanically-oriented observables such as lattice constants and internal friction.

Within these restrictions we have made every effort to be comprehensive. Our goal has been to gather into

arXiv:1805.10912v3 [cond-mat.dis-nn] 15 Jun 2019

one place all experimental data on characteristic temperatures above  $T_c$ .

We separate the results of distinct experimental groups into distinct data sets. When a group used several experimental techniques, identified several characteristic temperatures in their data, or re-analyzed data from other publications, we separate these distinct results into distinct data sets. When a group republished or revised their results, we use the latest results. Full details about each data set and about which papers did and did not match our selection criteria are included in the appendices.

## I. LSCO DATA

Figure 1 summarizes the experimental corpus on strontium-doped LSCO. While this compound has a relatively low maximum  $T_c$  of about 39 K, it is stable up to 1000 Kelvin and the full range of dopings across the cuprate superconducting dome can be explored. The corpus contains a total of twenty distinct data sets from thirteen distinct experimental groups published between 1990 to 2018, using a variety of sample preparation techniques and experimental probes developed over the decades. Five more data sets<sup>102</sup> exist on characteristic temperatures in neodymium and europium-doped LSCO, with excellent agreement with the strontium doped results shown here. Appendix B gives full details on each of these data sets and on three more strontium-doped data sets<sup>103</sup> which we have omitted on a case by case basis. In order to show the slope and profile of individual data sets we plot lines connecting the data points within each set.

Figure 1 shows that the data sets are in remarkable agreement, forming a pattern of four distinct characteristic temperatures which each start high at small doping and decrease as doping is increased. Despite the variety of samples and probes, the scatter in data points around each characteristic temperature is small, of order  $\pm 15$  K on the lowest three characteristic temperatures (orange, green, and blue lines), and somewhat larger on the highest characteristic temperature (red lines). Gaps which are much larger than this scatter separate each of the characteristic temperatures, allowing each data set to be unambiguously assigned to one of the four characteristic temperatures. We number characteristic temperatures from the top, with  $n = 1$  on the highest (red) line,  $n = 2$  on the next highest (orange), etc.

The topmost red lines (four data sets) show  $T_{max}$ , visible both as a peak in the magnetic susceptibility and as kinks in the resistance and thermoelectric power (TEP).<sup>44,64,99</sup> The yellow lines (second from the top, five data sets) show the temperature  $T_{LTO}$  of the well-known transition from the high symmetry tetragonal phase to a lower symmetry orthorhombic phase, which has generally though not unanimously<sup>83</sup> been regarded as simply a structural phase transition with little re-

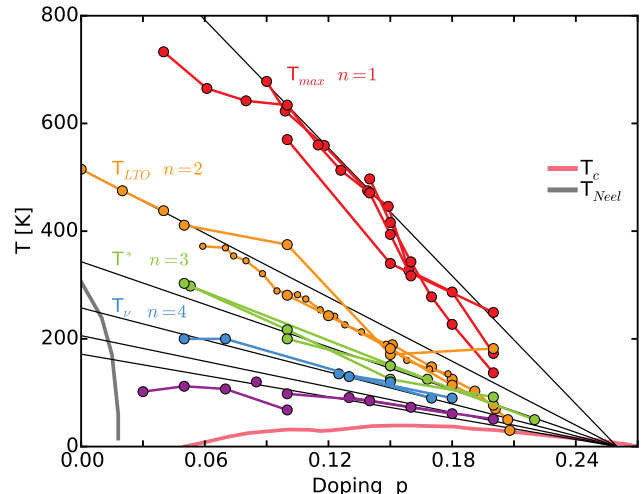


FIG. 1: (Color online.) The family of pseudogap lines in LSCO. The black guides to the eye have slopes proportional to  $1/n$  and meet at doping  $p = 0.26$ . Individual pseudogap data sets, each from a distinct experimental group measuring a distinct experimental probe and signature, are shown as filled circles connected by lines. The hallmark of the first (red) pseudogap line  $T_{max}$  is a peak in the magnetic susceptibility.  $C_4$  symmetry is broken on the second (orange) line  $T_{LTO}$ , and the ARPES density of states develops a pseudogap on the third (green) line  $T^*$ . The fourth pseudogap line  $T_v$  (blue) is marked by transport signatures. Purple lines show NMR, Hall angle, heat capacity, and neutron scattering data sets. The pink line shows the superconducting  $T_c$ . An antiferromagnetic phase (grey line) is found at low dopings.

lation to high  $T_c$ .<sup>2,42,44,83,97</sup> This transition manifests clearly in neutron scattering, X-ray diffraction, resistance, and TEP measurements. The green lines (third from the top, four data sets) mark the pseudogap temperature  $T^*$ , where ARPES shows that a pseudogap opens in the density of states. Like  $T_{max}$  and  $T_{LTO}$ ,  $T^*$  is seen also in the resistance and the TEP.<sup>2,28,44,58,98</sup> The blue lines (fourth from the top, three data sets) are a recently identified second pseudogap transition  $T_v$  visible in the Nernst effect and in nuclear magnetic resonance (NMR).<sup>16,25,37,89,96</sup> This transition is well attested by four additional Nernst and resistance data sets<sup>104</sup> in neodymium-doped and europium-doped variants of LSCO, which give temperatures that agree very well with the strontium-doped LSCO data.<sup>11,16</sup> We include also four NMR, Hall angle, heat capacity, and neutron scattering data sets (in purple) which suggest similar lines at lower temperatures.<sup>4,37,57,95</sup>

The fact that over the last thirty years experiments on LSCO's temperature dependence consistently have found distinctive behavior (peaks, kinks, extinction of diffraction peaks, etc.) on these four fairly crisp lines, and not in the intervening gaps, indicates that this pattern has predictive power. We expect that future experiments will continue to find smooth temperature dependence in the

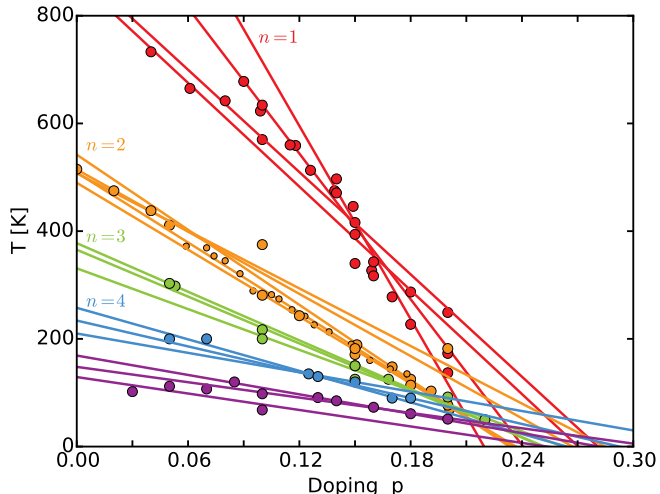


FIG. 2: (Color online.) Intersection of the pseudogap family in LSCO near  $T = 0$ ,  $p = 0.26$ . The straight lines show linear fits to individual pseudogap data sets, displayed as filled circles.

gaps and anomalous behaviors on these lines. This observed pattern and prediction are our most important results.

The four characteristic temperatures just discussed follow a pattern which we have highlighted with thin black lines.<sup>105</sup> Both the experimental data and the black lines are organized as harmonics of the uppermost line, with the  $n$ -th line having a slope equal to  $1/n$  times that of the highest  $n = 1$  line.<sup>106</sup> Moreover all four lines radiate from a point  $p \approx 0.26$  that lies near the high-doping limit  $p_{c2} = 0.27$ <sup>21</sup> of the superconducting dome. Figure 2 displays linear regressions of the eighteen pseudogap data sets which contain more than one data point. The linear regressions of fourteen out of eighteen pseudogap data sets intercept the  $T = 0$  axis in the interval  $p = [0.23, 0.29]$ , of which six lie in  $[0.25, 0.27]$ . These regressions place the pseudogap's  $T = 0$  intercept on or near the high-doping edge of LSCO's superconducting dome, and clearly exclude the possibility suggested by some that the intercept lies well inside the dome, near  $p = 0.19$ .<sup>68</sup>

Both the agreement of intercepts and the pattern of  $1/n$  slopes are remarkable given that we have used very broad selection criteria embracing an extremely diverse set of experimental techniques and sample preparation protocols, publications from 1990 to the present, and significant scatter within individual data sets. While it is often suggested that the pseudogap temperature is sensitive to the experimental technique, we find instead that all published measurements agree on the same simple pattern.

These results force the conclusion that all four characteristic temperatures are members of the same family. This family pervades most if not all of the cuprate

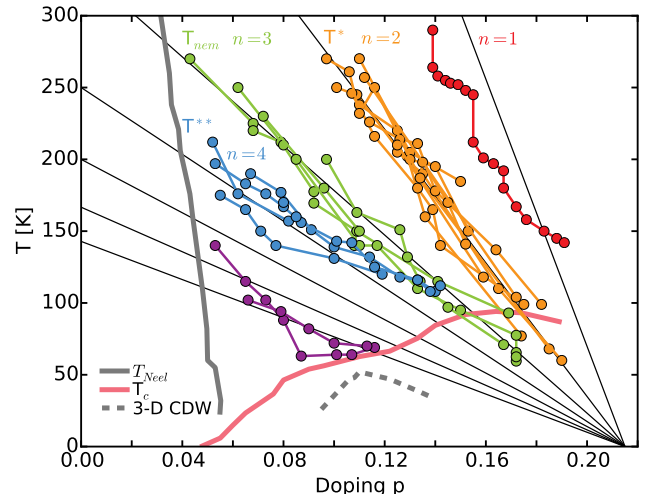


FIG. 3: (Color online.) The family of pseudogap lines in YBCO. The black guides to the eye have slopes proportional to  $1/n$  and meet at doping  $p = 0.215$ . Individual pseudogap data sets, each from a distinct experimental group measuring a distinct experimental probe and signature, are shown as filled circles connected by lines. Near the first  $n = 1$  pseudogap line a transport anomaly (red data set) occurs.  $C_4$  and intra unit cell symmetries are broken on the second (orange) line  $T^*$ , while on the third (green) line  $T_{nem}$  transport becomes nematic and time reversal symmetry is broken. The fourth pseudogap line  $T^{**}$  (blue) is marked by transport signatures. Purple lines show additional transport data sets. The pink line shows the superconducting  $T_c$ . Underneath  $T_c$  three-dimensional charge density wave order (dashed grey) occurs, and an antiferromagnetic phase (solid grey) is found at low dopings.

phase diagram: in LSCO the  $n = 2$  pseudogap line, i.e. the transition to orthorhombic symmetry, persists to zero doping and 515 K, and the  $n = 1$  pseudogap line extends to above 700 K. Since the  $n = 1$ ,  $n = 3$ , and  $n = 4$  lines in this family are not structural transitions, the tetragonal to orthorhombic structural symmetry breaking on the  $n = 2$  line must be a subsidiary signal of underlying electronic nematic order.

## II. YBCO DATA

Figure 3 summarizes the experimental data on oxygen doped YBCO. The experimental corpus contains a total of twenty-six distinct data sets from 1996 to 2018. Appendix C gives full details on each of these data sets, three more data sets which are in excellent agreement but which we have omitted because their data points show unusually large scatters<sup>107</sup>, and another data set which we have omitted on a case by case basis.<sup>108</sup>

Although oxygen doped YBCO has a considerably higher maximum  $T_c \approx 94$  K than LSCO, the data on its phase diagram is much curtailed. Hole dopings above

$p = 0.194$  cannot be obtained at ambient pressure, and the experimental literature on the pseudogap generally has not measured dopings less than  $p \leq 0.05$ , most likely because of proximity to the antiferromagnetic Neel phase, marked in grey in Figure 3. Whether this practice assumes or confirms that the pseudogap lines do not coexist with Neel order seems unclear. We have not collated characteristic temperatures on the calcium doped variant of YBCO, in which hole dopings well in excess of  $p = 0.194$  can be achieved, because much less experimental data is available on characteristic temperatures in this variant compound.

In the remaining doping range  $0.06 \leq p \leq 0.194$  we are able to clearly identify the  $n = 2$ ,  $n = 3$ , and  $n = 4$  pseudogap lines, which follow rays intersecting near  $p \approx 0.215$ .<sup>109</sup> The scatter of data around each characteristic temperature is about the same as in LSCO, of order 15 K. We find again clear gaps between the characteristic temperatures, allowing each data set to be unambiguously assigned to one of the characteristic temperatures.

The orange lines (ten data sets) show YBCO's pseudogap temperature  $T^*$ , marked by transport signatures and the onset of fluctuating intra unit cell order. Recent symmetry-oriented experiments show that this is a nematic  $C_4$  symmetry breaking transition similar to the symmetry breaking seen on LSCO's  $n = 2$  line. However these experiments go beyond the neutron scattering and X-ray diffraction experiments performed on LSCO, and find that  $C_2$ , mirror, and inversion symmetries are also broken in addition to  $C_4$  symmetry breaking.<sup>1-3,16,20,23,39,50,52,54,55,62,76,78,79,90,100,101</sup> On the green  $T_{nem}$  lines (seven data sets), transport becomes nematic and time reversal symmetry is broken.<sup>2,17,19,40,92</sup> The nematic temperatures  $T_{nem}$  have values equal to two thirds those of the pseudogap temperatures  $T^*$ , not one half. This is the reason why we assign  $n = 2$  to  $T^*$  rather than  $n = 1$ , and  $n = 3$  to  $T_{nem}$  rather than  $n = 2$ . At large dopings both the  $n = 2$   $T^*$  and  $n = 3$   $T_{nem}$  lines clearly cross the superconducting dome and coexist with the superconducting phase, excluding the possibility that the pseudogap transition merges with the superconducting phase transition rather than crossing it.<sup>68</sup> Next the blue  $T^{**}$  lines ( $n = 4$ , six data sets) have been measured in resistance and Hall resistance experiments, and their values are one half those of the pseudogap temperatures  $T^*$ , leading us to assign  $n = 4$  to the  $T^{**}$  lines.<sup>3,49,77</sup> At dopings  $p < 0.085$  intra unit cell ordering occurs on this  $n = 4$  pseudogap line rather than on the  $n = 2$  line.<sup>5,30,80</sup>

Turning to YBCO's  $n = 1$  pseudogap line, experiments have almost never explored temperatures above 300 K because of concerns about thermal history memory, aging and equilibration, and preparation protocol. This leaves only a small corner in the phase diagram where the  $n = 1$  line might be seen, stretching from  $p = 0.15$ ,  $T = 300$  K to  $p = 0.194$ ,  $T = 95$  K, which limits our ability to ascertain the existence of a line here. In this region there is a large step change in the resistance and an onset of ther-

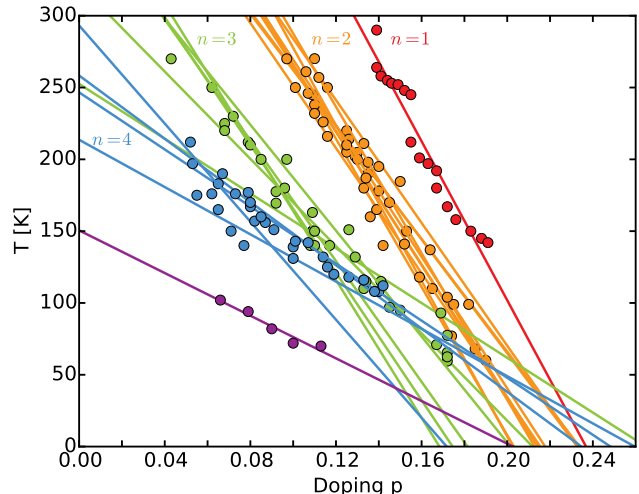


FIG. 4: (Color online.) Intersection of the pseudogap family in YBCO near  $T = 0$ ,  $p = 0.215$ . The straight lines show linear fits to individual pseudogap data sets, displayed as filled circles.

mal history memory<sup>48,63</sup>. Moreover Ando's resistance measurements show a prominent white contour, plotted in red in Figure 3, which is roughly aligned with the expected  $n = 1$  line.<sup>2</sup>

All four pseudogap lines intercept  $T = 0$  at doping  $p \approx 0.215$  with a scatter that is again notably small, comparable to the scatter around LSCO's  $p \approx 0.26$ . Figure 4 displays linear regressions of the twenty-two pseudogap data sets which contain more than one data point.<sup>110</sup> The linear regressions of fifteen out of twenty-two pseudogap data sets intercept the  $T = 0$  axis in the interval  $p = [0.20, 0.24]$ , and six are clustered in  $[0.21, 0.22]$ . Only four out of twenty-two of the intercepts are found at dopings less than  $p = 0.20$ , excluding the possibility that YBCO's pseudogap intercept lies near  $p = 0.19$ .<sup>68</sup>

### III. COMPARISON

Comparing LSCO to YBCO, the pseudogap lines extrapolate to zero-doping temperatures which are the same within experimental error, i.e. 515 K for LSCO's  $n = 2$  line vs. 500 K for YBCO.<sup>111</sup> However the pseudogap family's meeting point on the  $T = 0$  axis lies at considerably different dopings: in YBCO it lies at  $p \approx 0.215$ , while in LSCO it is found at  $p \approx 0.26$ . This should lay to rest debates about the  $T = 0$  intercept of the pseudogap line, and about the location of the putative quantum critical point: if the question is framed in terms of hole doping  $p$ , the answer clearly depends on the material. Yet the question can be answered in a different way that is not material dependent: in both LSCO and YBCO the pseudogap's  $T = 0$  intercept lies very near to the maximal doping  $p_{c2}$  at which superconductivity can be

achieved, which has two different values,  $p_{c2} = 0.27^{21}$  in LSCO vs.  $p_{c2} = 0.194^{51}$  in oxygen-doped YBCO at ambient pressure. In this sense the pseudogap lines in both LSCO and YBCO reach  $T = 0$  at the real material-dependent end of the superconducting phase. We conclude that in both materials the entire superconducting dome lives under the shelter of the pseudogap family, and that its overdoped edge is tied to the pseudogap.

The various observables marking the pseudogap family collapse at critical dopings which depend on the line, and the doping scheme<sup>11</sup>, and the observable. On LSCO's  $n = 1$  line the linear resistance signature collapses between  $p = 0.17$  and  $p = 0.18^{15,16,64}$ , while the peak in the magnetic susceptibility continues past  $p = 0.20^{64}$ . On the  $n = 2$  line the tetragonal phase associated with this line collapses near  $p = 0.208^{83}$ , and on the  $n = 3$  line the ARPES pseudogap persists until at least  $p = 0.22^{28}$ . It seems likely that the collapse of each line is caused by a small competing temperature scale, since in both LSCO and YBCO the  $n = 2$ ,  $n = 3$ , and  $n = 4$  lines either collapse or disappear from the experimental record between 50 and 110 K. The coupling between copper oxygen planes is a likely candidate for supplying the competing scale, since it supports long range 3-D charge density waves and superconductivity in roughly the same temperature range.

The experimental signatures associated with each of the pseudogap lines in YBCO could differ substantially from the signatures seen on corresponding lines in LSCO. Except for the  $n = 2$  line, comparisons of symmetry breaking in LSCO and YBCO are impossible because LSCO pseudogap experiments have generally not probed symmetry breaking. Moreover, the hallmark of LSCO's  $n = 3$  line is that the ARPES density of states begins to manifest a pseudogap, while in YBCO this change is generally believed to occur instead on YBCO's "pseudogap line" i.e. its  $n = 2$  line. Since there is no ARPES data on YBCO's pseudogap temperature, it remains possible that in YBCO the pseudogap could manifest in the density of states on the  $n = 3$  line rather than the  $n = 2$  line, the same as in LSCO. This question is confused further by data on  $p \approx 0.14$   $\text{Bi}_2\text{Sr}_2\text{CaCu}_2\text{O}_{8+\delta}$  (Bi2212) where the ARPES pseudogap seems to open in two discrete steps near  $T = 250$  K and  $T = 150$  K, suggesting that in Bi2212 the density of states may change substantially at two distinct pseudogap lines.<sup>87</sup>

#### IV. ANALYSIS

These results are very fertile ground. First, the fact that the pseudogap family spans all dopings up to  $p_{c2}$  and temperatures up to 700 K argues strongly that the entire phase diagram up to  $p_{c2}$  hosts a single mother phase or order. The various phenomena observed along the pseudogap lines, for instance the structural phase transition to orthorhombic order, are then subsidiary or parasitic phenomena that respond to underlying changes

in the mother phase. The details of which line a particular observable (such as orthorhombic symmetry) is associated with may depend on the material, and even when a particular observable in a particular material collapses at a particular doping the underlying line in the mother phase may continue robustly to higher dopings. As a case in point, in YBCO intra unit cell order switches from the  $n = 4$  line to the  $n = 2$  line near  $p = 0.085^{5,23,30,54,55,62,79,80}$ , while transport signals show that the  $n = 4$  line continues until at least  $p = 0.142^{3,49,77}$ . Superconductivity may also be a subsidiary or parasitic phenomenon which occurs when (a) the mother phase assists hole transport and (b) the interlayer coupling is strong enough to support long range 3-D order.

Secondly, the width of the pseudogap lines is unquestionably sharp compared to the pseudogap temperatures themselves. Figures 1 and 3 show that the scatter around each pseudogap line is typically of order  $\pm 15$  K.<sup>112</sup> This sharpness controverts the hypothesis that the pseudogap line is a crossover, and could be understood as evidence of standard phase transitions. However the fact that there is a family of repeated pseudogap lines indicates that we are instead seeing a quantum coherent effect in the mother phase, in the same category as Landau levels or atomic orbitals. If so, then quantum coherence must persist to temperatures as high as 700 K in the cuprates. This conclusion is reinforced by parallel evidence from the strange metallic (linear in magnetic field and linear in temperature) resistance seen in the cuprates, which is also a manifestation of quantum coherence at temperatures far above  $T_c$ .<sup>26,31,75</sup>

Thirdly, the pseudogap lines are in truth linear. Clarity about this linearity was obtained by restricting our data to single materials with a single doping scheme. There are some mild deviations from linearity - YBCO's  $n = 4$  pseudogap line flattens at around 140 K, and LSCO's  $n = 1$  and  $n = 2$  lines steepen at high dopings - but these are mild distortions, and are the exception rather than the rule. The pseudogap lines relate temperature  $T$  to the 2-D sheet density of holes  $\rho_{holes} = p/\mathcal{A}$  within the copper oxide plane. Here  $\mathcal{A}$  is the area of the copper oxide unit cell. Since in atomic units sheet density has the same units as both temperature and energy, we conclude that the pseudogap temperatures are direct measures of a sheet density. This conclusion is supported by the fact that in atomic units the constant of proportionality between the  $n = 1$  pseudogap line and  $\rho_{holes}$  is of order one:  $-1.27$  for LSCO and  $-1.55$  for YBCO. The natural endpoint of this reasoning is that in the cuprates there is a two dimensional sheet density  $\Pi_{psg}$  which controls both the pseudogap family and the family's mother phase, that  $\Pi_{psg} \propto p_{c2} - p$  is high at low dopings and decreases linearly to zero at  $p_{c2}$ , and that the pseudogap temperatures are direct measures of this density.

Two other linear relations between sheet density and temperature have already been seen in the cuprates. Uemura's proportionality relation between the superfluid

density and  $T_c$  holds in many underdoped materials<sup>86</sup>, and a formally identical relation has been verified also in overdoped LSCO<sup>9</sup>. Secondly, several LSCO and Bi2212 experiments have reported temperature scales which rise linearly with hole doping  $p$  and extrapolate to zero at the underdoped end of the superconducting dome, so that these temperatures seem to measure the sheet density of mobile holes - see Figure 6 in Appendix A for a summary of these results.<sup>10,29,44,72</sup> It is also significant that 3-D long range charge density wave (CDW) order and the 1/8-th anomaly occur near half-filling for  $\Pi_{psg}$ , suggesting that these may be favored when the pseudogap density is about one half of its maximum value.

It is technically possible that the pseudogap density  $\Pi_{psg}$  and pseudogap lines could reflect strictly ultraviolet i.e. short range physics near the atomic scale, and that the cuprate phase diagram is not controlled directly by  $\Pi_{psg}$  but instead through renormalization group flow from short range to long range collective behavior. This has the weaknesses that atomic scale physics would be expected to cause resonances in the phase diagram at values of  $\Pi_{psg}$  tied to the crystal structure, but these are not seen, and that at dopings near  $p_{c2}$  the area scale indicated by  $\Pi_{psg}^{-1}$  is far in excess of the atomic scale. In our view it is more likely that  $\Pi_{psg}$  is a fundamental determining property of long-range order in the pseudogap mother phase. We leave for future work the question of what quantity is counted by  $\Pi_{psg}$ , although some of the obvious possibilities are vortices, skyrmions, dislocations, entanglement density, or topological quantities.

Fourthly, we turn to the  $1/n$  quantization rule which controls the slopes. In this connection we are inspired by recent experimental and theoretical work which shows a direct linear relation between magnetic field  $B$  and temperature  $T$  in the strange metal phase of LSCO and other bad metals.<sup>26,31,45,75</sup> The pattern traced by the pseudogap family can be reproduced by a model of free two dimensional  $p^2/2m$  fermions where temperature is mapped to an effective magnetic field  $B$  and the pseudogap sheet density  $\Pi_{psg} \propto p_{c2} - p$  is mapped to a Fermi level  $E_F$ . As shown in Figure 5, if the effective model includes either a Berry phase<sup>59</sup> or a Zeeman term  $\mu_0 B \sigma_z$ , then its Landau levels have the same  $1/n$  slopes seen in the pseudogap family and intersect at a common point  $B = 0$ ,  $E_F = 0$ . This model leads us to the conjecture that the pseudogap family is in some way related to the Integer Quantum Hall Effect. Our conjecture is not a suggestion of well-defined quasiparticles or, going further, a Fermi liquid or band structure. Topology can control conduction even when these concepts are not relevant, as has been seen in studies of strongly disordered topological insulators.<sup>94</sup>

Figure 5 shows that the effective model possesses an additional  $n = 0$  Landau level at  $E_F = 0$ , which maps to a vertical line in the cuprate phase diagram at the upper critical doping  $p_{c2}$ . This prediction is confirmed in LSCO by three experimental signatures which are extinguished on this line: the superfluid density<sup>9</sup>, the electronic nematicity which is found at all lower dopings<sup>91</sup>,

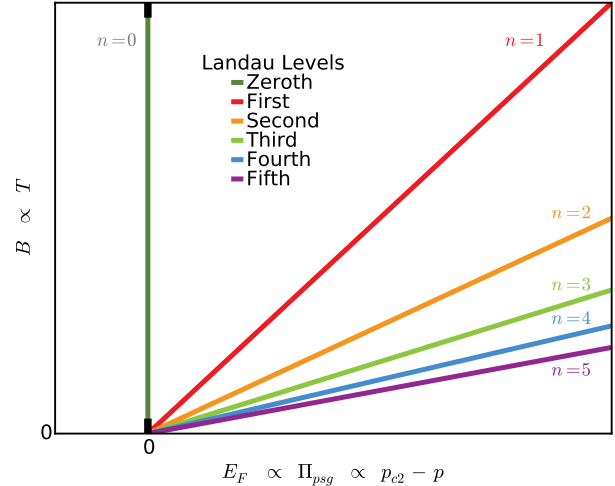


FIG. 5: (Color online.) Effective model producing the same pattern seen in the pseudogap family. The model describes free two-dimensional  $p^2/2m_e$  fermions with a Zeeman splitting  $\mu_0 B \sigma_z$  moving in a magnetic field  $B$ . We plot the resulting Landau levels with their energies  $E_n$  along the  $x$  axis and with magnetic field  $B$  along the  $y$  axis. The Landau level slopes follow the same  $1/n$  pattern seen in the pseudogap family if field  $B$  is mapped to temperature and Fermi energy  $E_F$  is mapped to pseudogap density  $\Pi_{psg}$ .

and the coefficient of the linear-in-temperature contribution to the resistivity<sup>21,33</sup>.

In summary, we have shown that the experimental corpus on cuprate characteristic temperatures shows that signals such as peaks, kinks, or extinction of diffraction peaks are found on four pseudogap lines which span the cuprate phase diagram. In the large gaps between the four lines no such signal is found and temperature dependence is smooth. This observation is also a prediction about future measurements of cuprate characteristic temperatures. We have argued that the entire cuprate phase diagram from zero doping out to  $p_{c2}$  hosts a single mother phase which is controlled by a two dimensional sheet density, and that the observed family of pseudogap lines are subsidiary phenomena caused by changes in the mother phase. We also suggest that the superconducting phase and charge density wave order are supported by the mother phase and occur when it is augmented with an interplane coupling and, in the case of superconductivity, with hole carriers.

## Appendix A: Temperature scales that rise proportionally to hole doping

With the exception of Refs.<sup>36,73</sup>, the data sets graphed in Figure 6 are temperatures that rise linearly with doping and extrapolate to  $T = 0$  near the underdoped limit of the superconducting dome, i.e. in the interval  $p = [0.049, 0.081]$ . This suggests that these temperatures are direct manifestations of the sheet density of mobile holes. Ref.<sup>36</sup> reports an energy scale with a similar behavior.

Ref.<sup>73</sup> also reports a temperature which rises linearly up to  $T = 300$  K. This last data set extrapolates to  $T = 0$  at a lower doping  $p = 0.023$ , presumably because of a sensitivity to pinned holes.

All data sets used in Figure 6, with discussion of their particulars and origin, and with a script that produces this figure, are available in the supporting material as a python script.

1. Hashimoto, 2009.<sup>29</sup> Angularly integrated ARPES. LSCO. The authors take the first derivative of the spectrum with respect to energy, and identify a peak in the first derivative. The temperature reported here, which they call a coherence temperature, is a break in the temperature dependence of the peak position. We omit a data point at  $p = 0.15$  which fits well with the linear regression because they did not actually reach the reported temperature  $T = 364$  K. Roughly consistent with Ref.<sup>36</sup>. The slope is 6200 K without the  $p = 0.15$  data point, or 4900 K with it.
2. Ino, 2009.<sup>36</sup> Angularly integrated ARPES. LSCO. The quantity reported here is a measure of the width of the Fermi surface. Unlike all other data discussed in this article, this is an energy scale converted to temperature, not an experimental temperature. The experiment was performed at  $T = 18$  K. The quantity reported here includes a factor of  $1/\pi$  which might be able to be renormalized at will. We include this data set because the four data points between  $p = 0.074$  and  $p = 0.203$  rise linearly with doping and extrapolate to the underdoped edge of the superconducting dome. We omit the  $p = 0.30$  point from the linear fit, and we omit the  $p = 0$  point altogether because Figure 2 in Ref.<sup>36</sup> shows  $p = 0$  data that seems to leave little ground for extracting a width. The slope is 4600 K.
3. Kim, 2004.<sup>44</sup> Thermoelectric power. LSCO. The temperature reported here marks a break from the linear signal seen at high temperatures. Here we plot only the dopings at  $p = 0.20$  and higher. The slope is 2100 K, about half of the slope in Ref.<sup>36</sup>.
4. Chatterjee, 2011.<sup>10</sup> ARPES. Bi2212. Below this temperature the spectrum contains a sharp Gaussian peak, and above this temperature the peak is

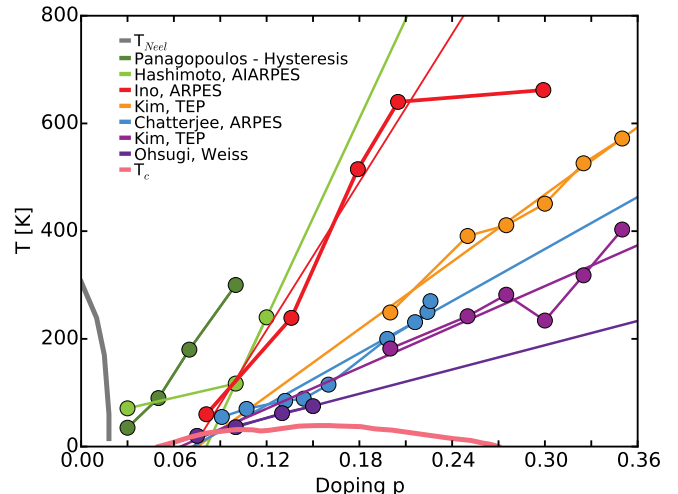


FIG. 6: (Color online.) Characteristic temperatures that seem to be direct manifestations of the density of mobile holes. Light green, red, and blue data sets were measured using ARPES, yellow and light purple sets with the thermoelectric power, and the dark purple data set with the magnetic susceptibility. The dark green set measuring the onset of magnetic hysteresis intercepts the  $p$  axis at lower doping, perhaps because it is sensitive to pinned holes. The superconducting dome is shown in pink, and the antiferromagnetic phase in grey.

absent. Unlike all other data discussed in this article, this data is obtained from Bi2212.

5. Kim, 2004.<sup>44</sup> Thermoelectric power. LSCO. The temperature reported here marks a break from the linear signal seen at low temperatures. Here we plot only the dopings at  $p = 0.20$  and higher.
6. Ohsugi, 1991.<sup>72</sup> Nuclear quadrupole resonance. LSCO. The temperature reported here is a Weiss temperature obtained by fitting the nuclear spin relaxation rate to a Curie-Weiss law.
7. Panagopoulos, 2006.<sup>73</sup> See also Ref.<sup>74</sup> by the same group. LSCO. This temperature marks the onset of hysteresis in the temperature dependence of the low field magnetization, which is probably a sign of pinned vortices and of pairing. The low-doping data from  $p = 0.03$  to  $p = 0.10$  nicely follows a straight line originating at  $T = 0$ ,  $p = 0.023$  and extending up to room temperature. The small  $p = 0.023$  intercept may be caused by the observable's sensitivity to both pinned and mobile holes. The slope is about 3900 K, roughly comparable to the slopes of the LSCO ARPES data sets.<sup>29,36</sup>

## Appendix B: LSCO Data Sets

The temperatures gathered here were all realized experimentally rather than by extrapolation from lower temperatures, and clearly identifiable signals occurred at the reported temperatures, including peaks, kinks, extinction of diffraction peaks, etc. In the interest of clarity we do not rely on universality arguments, and therefore restrict ourselves to lanthanum cuprate with strontium doping(LSCO), and we keep separate the results of distinct experimental groups and of distinct experimental probes and signatures. We do not report any temperatures that are not already reported by the articles we have cited. In particular, we have stayed out of the business of re-analyzing or fitting data sets from other articles. The one exception to this rule is our use of the color maps in<sup>2</sup> - from that article we extracted data from certain contours and features that are prominent in the color maps.

Our survey of pseudogap temperature measurements does not extend to the extensive literature on anomalies and phase transitions measured using mechanically-oriented observables such as internal friction, sound velocity, lattice constants, thermal expansivity, and the like.<sup>22</sup>

All data sets used in the LSCO figures or enumerated here, with discussion of their particulars and origin, and with a script that produces the figures, are available in the supporting material as a python script.

1.  $n = 1$  line: In LSCO the  $n = 1$  line marks a resonance in the magnetic susceptibility and qualitative changes in transport and in the thermoelectric power.
  - (a) Yoshizaki, 1990.<sup>99</sup> Peak in the magnetic susceptibility.
  - (b) Nakano, 1994.<sup>64</sup> Peak in the magnetic susceptibility. The peak continues past  $p = 0.20$ , and disappears near  $p = 0.22$ . We omit the last three data points because no peak exists in those susceptibility curves until a Curie term has been subtracted. We also omit the first four data points, at lowest doping, because the experimental temperature did not go high enough to see the actual peak. The scaling analysis used to obtain those four points is however very convincing, especially because the peak was seen at lower dopings by<sup>99</sup>.
  - (c) Kim, 2004.<sup>44</sup> Thermoelectric power. The temperature reported here marks a break from the linear signal seen at high temperatures. Here we plot only the dopings up to  $p = 0.20$ .
  - (d) Nakano, 1994.<sup>64</sup> Resistivity. The temperature reported here marks a break from the linear signal seen at high temperatures. The break disappears and the signal seems to be perfectly linear (from visual inspection) at  $p = 0.16$  and  $p = 0.18$ , which is consistent with Ref.<sup>15</sup>'s
2.  $n = 2$  line: In LSCO the  $n = 2$  line is a symmetry breaking transition from  $C_4$  down to  $C_2$  nematic order. It has been commonly regarded as a structural transition from tetragonal to orthorhombic symmetry. It is accompanied by features in transport and in the thermoelectric power.
  - (a) Kim, 2004.<sup>44</sup> Thermoelectric power. The temperature reported here marks a break from the linear signal seen at low temperatures.
  - (b) Takagi, 1992.<sup>83</sup> X-ray diffraction, looking for a peak splitting caused by orthorhombicity. This data shows that the signal i.e. the orthorhombic phase collapses near  $p = 0.208$ . Our linear fit omits two points dropping almost vertically near  $p=0.208$ .
  - (c) Ando, 2004. Resistivity.<sup>2</sup> We reproduce a red linear feature that is very prominent in Ando's plot. The feature disappears in the range between  $p = 0.178$  and  $p = 0.19$ .
  - (d) Yamada, 1998.<sup>97</sup> Neutron scattering sensitive to orthorhombic symmetry.
  - (e) Keimer, 1992.<sup>42</sup> Neutron scattering sensitive to orthorhombic symmetry. More specifically, extinction of the (021) superlattice reflection peak.

data at  $p = 0.17, 0.18$ . This is also consistent with Ref.<sup>16</sup>'s statement that the resistivity signal of the pseudogap collapses between  $p = 0.17$  and  $p = 0.18$ .

There is apparent disagreement between Ref.<sup>64</sup> and Ref.<sup>46</sup>, which was cited by Ref.<sup>16</sup> by the same authors. Ref.<sup>64</sup> reports that at  $p = 0.14$  and  $p = 0.16$  the pseudogap temperature, i.e. the onset of linear in temperature resistance, occurs at 471 K and 317 K respectively. In contrast Ref.<sup>46</sup> gives resistivity data at  $p = 0.136, 0.143, 0.157, 0.163$  that superficially indicates much smaller temperatures. The  $p = 0.136$  resistivity seems to be linear above 150 K or so, and the  $p = 0.143$  resistivity seems to be linear above 110 K. However Ref.<sup>46</sup>'s data goes up to only 200 K, so they are unable to detect any linearity above 471 K. In contrast, Ref.<sup>64</sup>'s data at  $p = 0.14$  extends up to 900 K. Moreover, Ref.<sup>64</sup>'s data extends down to the superconducting temperature, shows that the slope below 471 K is not very different from the slope above that temperature, and changes only gradually. Therefore Ref.<sup>46</sup> may just not have enough data to detect nonlinearity near the high end of their temperature range. A second alternative is that there could be two linear regimes, one above 471 K, and another above 110 - 140 K, corresponding to two pseudogap temperatures.

3.  $n = 3$  line: In LSCO the  $n = 3$  line, also called the pseudogap temperature, is marked by the birth of a pseudogap controlling the density of states. It is accompanied by features in transport and in the thermoelectric power.

- (a) Yoshida, 2012.<sup>98</sup> ARPES. The data here is the temperature where the pseudogap (measured with ARPES) disappears.
- (b) Ando, 2004.<sup>2</sup> Resistivity. We reproduce a line segment imposed on the data by the authors which follows qualitative trends of the colors in their graph. We omit the first of the two line segments which they imposed, a constant-temperature  $T = 298$  K line at low doping  $p \leq 0.053$ . This  $T = 298$  K line is in fact supported by colors in the graph. At the overdoped end, the authors' line continues to  $p = 0.168$ ,  $T = 125$  K, but the underlying resistivity data suggests that the line should stop a little earlier, between  $p = 0.15$  and  $p = 0.168$ .
- (c) Kim, 2004.<sup>44</sup> Peak in the thermoelectric power. Here we plot only the dopings from  $p = 0.05$  up to  $p = 0.20$ . At higher dopings the signal increases very slowly with doping.
- (d) Hashimoto, 2007.<sup>28</sup> Angularly integrated ARPES. At temperatures below this temperature the density of states increases relatively rapidly with temperature, and above this temperature the DOS increases less quickly with temperature - i.e. the slope changes from one value to another in a discontinuous way. We omit a zero temperature data point at  $p=0.30$  because it only bounds the doping value where this line collapses to the range between  $p = 0.22$  and  $p = 0.30$ . We also omit the  $p = 0.03$ ,  $T = 300$  K data point because here no break is observed in the data, i.e. there is no data above 300 K. This pseudogap temperature is based on the authors noticing that at other dopings the slope below  $T^*$  decreases inversely with  $T^*$ , as seen in the inset of their Figure 2a. This  $p = 0.03$  data point agrees very well with all other data points on this line, and extends the line down to  $p = 0.03$ .
- (e) Matt, 2015.<sup>58</sup> ARPES. Based on measurements of the normal-state antinodal spectral gap -  $T^*$  is the temperature where this gap goes to zero. This data point is omitted because it concerns Nd-LSCO, but it does match the  $n = 3$  line well. They also show a strong pseudogap at  $p = 0.12$  which results in a bound  $T^* > 75$  K, though probably  $T^*$  is much larger than 75 K.

4.  $n = 4$  line: In LSCO the  $n = 4$  line is marked by features in transport and in nuclear magnetic

resonance.

We plot only the first three data sets listed here. The same pseudogap line revealed by these three data sets is very well supported by resistivity and Nernst data from Nd-LSCO and Eu-LSCO, as documented in the remaining data sets. All resistivity and Nernst data sets are shown together in Ref.<sup>16</sup> and show impressive agreement.

- (a) Cyr-Chinoire, 2018 re-analyzes Fujii, 2010.<sup>16,25</sup> Nernst effect. The temperature reported here marks a break from the linear signal seen at high temperatures.
- (b) Cyr-Chinoire, 2018 re-analyzes Ong, 2010/2011.<sup>16,89,96</sup> Nernst effect. The temperature reported here marks a break from the linear signal seen at high temperatures. This data set is a re-analysis of Nernst effect data from two papers which have Wang, Xu, Ong, and Uchida as co-authors.
- (c) Itoh, 2004.<sup>37</sup> NMR. Peak in the nuclear spin-lattice relaxation rate.
- (d) Cyr-Choiniere, 2018.<sup>16,18,25</sup> Nernst effect. The temperature reported here marks a break from the linear signal seen at higher temperatures. This data set of three data points from  $p = 0.15$  to  $p = 0.21$  is omitted because it concerns Nd-LSCO, but it matches the LSCO  $n = 4$  line well. It includes one data point from Ref.<sup>25</sup>. It also includes two data points from Cyr-Choiniere's Ref.<sup>18</sup>. A third  $p = 0.24$  data point from Cyr-Choiniere is not included in the data set (a double omission) because it lies at  $T = 0$  and therefore it only bounds the doping value rather than fixing it - however this data point does show that in Nd-LSCO this pseudogap line collapses somewhere between  $p = 0.21$  and  $p = 0.24$ .
- (e) Collignon, 2017.<sup>11</sup> Resistivity. The temperature reported here marks a break from the linear signal seen at higher temperatures. This data set from  $p = 0.20$  to  $p = 0.24$  is omitted because it concerns Nd-LSCO, but it matches the  $n = 4$  line well. When fitting to a straight line, we (doubly) omit a  $T = 0$  data point at  $p = 0.24$ . The pseudogap temperature at  $p = 0.23$  is 40 K, so the pseudogap temperature collapses to zero between  $p = 0.23$  and  $p = 0.24$ .
- (f) Collignon, 2017, analyzes Ichikawa, 2000.<sup>11,35</sup> Resistivity. The temperature reported here marks a break from the linear signal seen at higher temperatures. This data set from  $p = 0.12$  to  $p = 0.15$  is omitted because it concerns Nd-LSCO, but it matches the  $n = 4$  line well. This data set is two data points obtained by re-analyzing data from Ichikawa.

(g) Cyr-Chinoire, 2018.<sup>16,18</sup> Nernst effect. The temperature reported here marks a break from the linear signal seen at higher temperatures. This data set from  $p = 0.08$  to  $p = 0.21$  is omitted because it concerns Eu-LSCO, but it matches the LSCO  $n = 4$  line well. One data point within this data set is obtained from re-analysis of work from separate authors, so we (doubly) omit it. Three data points are from Ref.<sup>16</sup> and one data point is from Ref.<sup>18</sup> by the same authors.

#### 5. Other Data Sets:

- (a) Baledent, 2010.<sup>4</sup> Neutron scattering detecting intra unit cell two-dimensional short range order. This data point lies 4K above the  $n = 6$  line, well within experimental error bars.
- (b) Itoh, 2004.<sup>37</sup> NMR. A minimum in the nuclear spin-lattice relaxation rate. This data set looks like it could belong to the 5th or  $n = 6$  line.
- (c) Xu, 2000.<sup>95</sup> Tangent of the Hall angle. The temperature reported here marks a break from a quadratic form which gives a good fit at higher temperatures. We omit a data point which lies at  $T = 0$ ,  $p = 0.17$  because it only bounds the doping value where this temperature goes to zero to the interval between  $p = 0.10$  and  $p = 0.17$ .
- (d) Matsuzaki, 2004.<sup>57</sup> Peak in the heat capacity divided by temperature. This data set lies near the  $n = 5$  and  $n = 6$  lines.

#### 6. Superconducting $T_c$ and Neel temperature:

- (a) Momono, 1994.<sup>61</sup>  $T_c$ .
- (b) Ando, 2004.<sup>2</sup>  $T_c$ .
- (c) Doiron-Leyraud, 2009.<sup>21</sup>  $T_c = 0$  at  $p = p_{c2} = 0.27$ .
- (d) Keimer, 1992.<sup>41</sup> Neel temperature measured with neutron scattering.
- (e) Matsuda, 2002.<sup>56</sup> Neel temperature measured with neutron scattering.
- (f) Niedermayer, 1998.<sup>66</sup> Neel temperature measured with muon spin rotation.

#### 7. Omitted Data Sets:

- (a) Panagopoulos, 2004, 2005, 2006.<sup>53,73,74</sup> Onset of hysteresis in the temperature dependence in the low field magnetization. We omit these data sets because they are clearly not related to the pseudogap family. They are look like a high-temperature replica of the superconducting dome, reaching a maximum  $T \approx 300$  K, and cut across the  $n = 2$  line and all lower lines.

- (b) Oda, 1990.<sup>69</sup> Peak in the magnetic susceptibility. We omit this data set because it seems have been superseded by Ref.<sup>64</sup> by the same authors.
- (c) Oda, 1990.<sup>71</sup> Peak in the magnetic susceptibility. We omit this data set because it duplicates data in Ref.<sup>69</sup> by the same authors.
- (d) Oda, 1991.<sup>70</sup> Peak in the magnetic susceptibility. We omit this data set because it seems to have been superseded by Ref.<sup>64</sup> by the same authors. It does indicate that the peak disappears between  $p = 0.19$  and  $p = 0.21$ .
- (e) Momono, 1996.<sup>60</sup> Peak in the magnetic susceptibility. We omit this data set because it seems to duplicate data in Ref.<sup>64</sup>, which was published in the same year by the same authors.
- (f) Nakano, 1998.<sup>65</sup> Peak in the magnetic susceptibility. We omit this data set because five out of six data points are the same as Ref.<sup>64</sup> by the same authors, but divided by 4.3 in order to map to an energy scale.
- (g) Nakano, 1998.<sup>65</sup> Magnetic susceptibility. The temperature reported marks a break from the linear form seen at high temperatures. We omit this data set because it is the same as the susceptibility data in Ref.<sup>64</sup> by the same authors, divided by 4.3 in order to map to an energy scale.
- (h) Nakano, 1998.<sup>65</sup> Resistivity. We omit this data set it is roughly a factor of six smaller than the resistivity data in Ref.<sup>64</sup> by the same authors. The authors probably divided this data by some number to map to an energy scale, just as they did with the magnetic susceptibility data.
- (i) Hwang, 1994.<sup>34</sup> Hall resistance. We omit this data set because the method used to obtain it seems to allow for renormalization of the entire data set by a somewhat arbitrary multiplicative factor.
- (j) Batlogg, 1994.<sup>6</sup> Hall resistance. We omit this data set because the method used to obtain it seems to allow for renormalization of the entire data set by a somewhat arbitrary multiplicative factor. The authors are the same as in Ref.<sup>34</sup> and the Hall resistance data looks the same too. However here the data are limited to  $p = 0.15$  and higher while the other article includes five additional dopings that are less than  $p = 0.15$ .
- (k) Batlogg, 1994.<sup>6</sup> Reanalysis of Yoshizaki's magnetic susceptibility data, looking for a shoulder rather than a peak. We omit this data set because for the two highest doping

data points the shoulder is hard to identify and because at the four lower doping data points the physical meaning of the shoulder is not clear, since it remains to be seen whether there is actually a peak at those dopings.

- (l) Batlogg, 1994.<sup>6</sup> Resistivity - "changes of the high temperature slope curves." We omit this data set because it is only at lower dopings and its mathematical and physical meaning, i.e. the precise experimental meaning of "changes of the high temperature slope curves", is not clear.
- (m) Tallon, 1999, analyzes Boebinger, 1996.<sup>8,85</sup> Resistivity. We omit this data set because the method used to obtain it seems to allow for renormalization of the entire data set by an arbitrary multiplicative factor.
- (n) Johnston, 1989.<sup>38</sup> Peak in the magnetic susceptibility. While this paper is distinguished by being perhaps the first to notice a spin pseudogap, only three data points concern strontium doped LSCO. Of these three points, only one is from data that actually showed a peak in the susceptibility. We omit the remaining data point.
- (o) Takemura, 2000, analyzes Nishikawa, 1994.<sup>67,84</sup> Thermoelectric power, analyzed with a universal scaling method. We do not plot this data because the temperature reported here lies in the tail of the universal scaling curve and is not associated with any clear feature. On the other hand the results here are roughly the same as those produced by<sup>44</sup>'s thermoelectric power experiment, which used the onset of a linear signal to define their characteristic temperature.
- (p) Startseva, 1999.<sup>82</sup> Optical reflectivity and conductivity. We omit this data because there are only two data points at dopings separated by only 0.01 (probably close to the error bars in doping), and because the difference in temperature is very large: 50 K.
- (q) Wang, 2006.<sup>88</sup> Nernst effect. The temperature reported here marks a break from the linear signal seen at higher temperatures. We omit this paper and several others by the same group because their data has recently been questioned and re-interpreted by Ref.<sup>16</sup>.

### Appendix C: YBCO Data Sets

The temperatures gathered here were all realized experimentally rather than by extrapolation from lower temperatures, and clearly identifiable signals occurred at

the reported temperatures, including peaks, kinks, extinction of diffraction peaks, etc. In the interest of clarity we do not rely on universality arguments, and therefore restrict ourselves to oxygen doped YBCO, and we keep separate the results of distinct experimental groups and of distinct experimental probes and signatures. We do not report any temperatures that are not already reported by the articles we have cited. In particular, we have stayed out of the business of re-analyzing or fitting data sets from other articles. The one exception to this rule is our use of the color maps in Ref.<sup>2</sup> - from that article we extracted data from certain contours and features that are prominent in the color maps.

Our survey of pseudogap temperature measurements does not extend to the extensive literature on anomalies and phase transitions measured using mechanically-oriented observables such as internal friction, sound velocity, lattice constants, thermal expansivity, and the like.<sup>22,63</sup> Nor did we explore the extensive literature on hysteresis in YBCO and associated onset temperatures, or on oxygen movement and ordering.

When the hole doping was not reported, we used Ref.<sup>51</sup> to map from oxygen content (or, in one case, from  $T_c$ ) to hole doping.

All data sets used in the YBCO figures or enumerated here, with discussion of their particulars and origin, and with a script that produces the figures, are available in the supporting material as a python script.

1.  $n = 1$  line:

- (a) Ando, 2004. Resistivity.<sup>2</sup> We reproduce a white contour that is prominent in Ando's data and starts near  $p = 0.140$ ,  $T = 291$  K.

2.  $n = 2$  line: In YBCO the  $n = 2$  line is marked by broken  $C_4$ ,  $C_2$ , mirror, and inversion symmetries, by fluctuating intra unit cell order which includes time reversal symmetry breaking, by a new contribution to nematic ordering, and by signatures in transport and in crystal vibrational frequencies. Several of the symmetry breaking signatures drop to the  $n = 4$  line at dopings lower than  $p < 0.085$ .

For this line only we omitted data sets which, compared to their linear regressions, showed a scatter of more than 10 to 15 K.

- (a) Zhang, 2018.<sup>100</sup> Muon spin relaxation. At temperatures below this temperature the spin relaxation reflects the existence of a slowly fluctuating magnetic field consistent with the intra unit cell order seen by neutron scattering, while above this temperature the field is absent. The entirety of this data is contested by Ref.<sup>81</sup> and a reply to that is contained within Ref.<sup>100</sup>.
- (b) Sato, 2017.<sup>76</sup> Torque magnetometry measurements of the anisotropic susceptibility. Above this temperature the anisotropy is a linearly

- increasing function of temperature, while below this temperature it begins increasing as temperature decreases. This signals that at the pseudogap a new contribution to nematic order is added.
- (c) Zhao, 2016.<sup>101</sup> Linear and  $n = 2$  line optical anisotropy. Below this temperature the  $n = 2$  line appears, signaling loss of inversion and  $C_2$  two-fold rotation symmetries. This is a stronger symmetry breaking than either nematic order or orthorhombic symmetry.
  - (d) Zhao, 2016, analyzes Lubashevsky, 2014.<sup>52,101</sup> Optical birefringence. The temperature reported here marks the onset of a polarized signal seen at lower temperatures, which signals loss of both mirror and  $C_4$  four-fold rotation symmetries.
  - (e) Sidis-Bourges, 2006-2015.<sup>5,23,54,55,62,79</sup> Polarized neutron scattering showing the onset of intra unit cell order, i.e. time reversal symmetry breaking while retaining lattice translational symmetry. Thirteen points from six different papers. The lowest doping data point, at  $p = 0.08$ ,  $T = 170$  K, lies near the  $n = 4$  line (about 13 K higher, within the published error bars of  $\pm 30$  K), while the other twelve points at higher dopings lie on the  $n = 2$  line. We omit this because the data set shows a scatter (compared to its linear regression, and not including the  $p = 0.08$  data point) of 30 K, which is above our cutoff.
  - (f) Daou, 2018/2010, analyzes Ando, 2004.<sup>2,16,20</sup> Resistivity. The temperature reported here marks a break from the linear signal seen at higher temperatures. We omit the  $p = 0.18$  data point on a specially irradiated sample in Ref.<sup>16</sup>.
  - (g) Arpaia, 2018.<sup>3</sup> Thin film on an MgO substrate. Resistivity. The temperature reported here marks a transition to linearity at higher temperatures.
  - (h) Arpaia, 2018.<sup>3</sup> Thin film on an SrTiO<sub>3</sub> substrate. Resistivity. The temperature reported here marks a transition to linearity at higher temperatures.
  - (i) Alloul, 2010.<sup>1</sup> Resistivity. The temperature measured here marks a transition to the linear resistivity seen at higher temperatures. We omit the  $p = 0.169$  data point because the sample has been irradiated to produce more disorder.
  - (j) Wang, 2017.<sup>90</sup> Resistivity. The temperature recorded here marks the transition to quadratic behavior at low temperatures.
  - (k) Kabanov, 1999.<sup>39</sup> Thin films on MgO and SrTiO<sub>3</sub>. Photoinduced transmission. The temperature measured here marks the end of a low temperature plateau in  $\delta T/T$ , where  $T$  is the photoinduced transmission signal. We omit this because the data shows a scatter (compared to its linear regression) of 30 to 40 K, which is above our cutoff.
  - (l) Leridon, 2009.<sup>50</sup> First derivative of the magnetic susceptibility with respect to temperature. At temperatures above this temperature the derivative is a decreasing function of  $T$ , while at lower temperatures it reverses its behavior and begins decreasing as  $T$  is reduced. We omit this data set because the data shows a scatter (compared to its linear regression) of 30 to 40 K, which is above our cutoff.
  - (m) Shekhter, 2013.<sup>78</sup> Resonant ultrasound spectroscopy measuring crystal resonance frequencies. At this temperature a sharp anomaly is seen in the resonance frequency and its slope changes abruptly. The width of the anomaly is 3 K, which is far sharper than any other data set on the pseudogap.
- It is worth noting that, unlike the other pseudogap signatures discussed in this article which focus on electronic response, resonant ultrasound spectroscopy is a probe of ionic motion. As such it belongs to the extensive cuprate literature on mechanically-oriented observables such as internal friction, sound velocity, lattice constants, thermal expansivity, oxygen movement, thermal history dependence, and the like.<sup>22,63</sup> It is extremely well attested that these observables reveal many distinct anomalies and phase transitions in the temperature range between  $T_c$  and room temperature. These features, their dependence on doping, and their qualitative behavior are not yet well understood. In this connection Ref.<sup>14</sup> has contested Ref.<sup>78</sup>'s pseudogap data in its entirety.
3.  $n = 3$  line: In YBCO the  $n = 3$  line is marked by time reversal symmetry breaking, onset of a spin resonance, and a new contribution to nematic order as seen in transport.
    - (a) Kapitulnik, 2009.<sup>40</sup> This temperature marks the onset of the Kerr effect, signaling time reversal symmetry breaking. We omit the data point at  $p = 0.156$  because it has an enormous 87 K error bar.
    - (b) Xia, 2008.<sup>93</sup> Polar Kerr effect. This temperature marks the onset of the Kerr effect, signalling time reversal symmetry breaking. They also find hysteresis at these temperatures, up to room temperature, indicating that time reversal symmetry breaking occurs also up to room temperature. We omit this data

- set because three out of four data points are repeated in<sup>40</sup> by the same authors.
- (c) Dai, 1999.<sup>19</sup> Neutron scattering. The temperatures recorded here mark the onset of a magnetic resonance which is measured by integrating the magnetic structure factor over momentum and frequency.
  - (d) Cyr-Choiniere, 2015.<sup>17</sup> Nematic component of the Nernst effect. The temperature recorded here marks a transition from steeply decreasing behavior (at low T) to slowly increasing linear behavior (at higher T). The authors argue that this marks the onset of a new contribution to the nematicity, and that this contribution is distinct from the nematicity at higher dopings which may be associated with charge density waves.
  - (e) Cyr - Choiniere, 2015, analyzes Ando, 2004.<sup>2,17</sup> Nematic component of the resistivity. They plot the ratio  $\rho_a/\rho_b$ , where  $\rho_a$  and  $\rho_b$  are measured along two different axis. The temperature recorded here marks a transition from steeply decreasing behavior (at low T) to slowly increasing linear behavior (at higher T). The authors argue that this marks the onset of a new contribution to the nematicity, and that this contribution is distinct from the nematicity at higher dopings which may be associated with charge density waves.
  - (f) Cyr - Choiniere, 2015.<sup>17</sup> Nematic component of the resistivity. They plot the ratio  $\rho_a/\rho_b$ , where  $\rho_a$  and  $\rho_b$  are measured along two different axis. The temperature recorded here marks a transition from a steeply decreasing behavior (at low T) to slowly increasing behavior (at higher T). The authors argue that this marks the onset of a new contribution to the nematicity, and that this contribution is distinct from the nematicity at higher dopings which may be associated with charge density waves.
  - (g) Wuyts, 1996.<sup>92</sup> Resistivity. They take the derivative of the resistivity with respect to temperature, find a peak in the derivative, and the peak position is the temperature recorded here. They originally multiplied by two and we remove that factor.
4.  $n = 4$  line: In YBCO the extent of the  $n = 4$  line, from  $p = 0.053$  to  $p = 0.142$ , is attested to by three transport data sets.
- (a) Arpaia, 2018.<sup>3</sup> Thin film on an MgO substrate. Resistivity. The temperature reported here marks a transition from quadratic at lower temperatures. Data from  $p = 0.053$  to  $p = 0.142$ .
  - (b) Arpaia, 2018.<sup>3</sup> Thin film on an SrTiO<sub>3</sub> substrate. Resistivity. The temperature reported here marks a transition from quadratic at lower temperatures. Data from  $p = 0.067$  to  $p = 0.140$ .
  - (c) LeBouef, 2011, analyzes Segawa, 2004.<sup>49,77</sup> Hall resistance. This temperature records the point where the second derivative of the Hall resistance changes sign. Data from  $p = 0.055$  to  $p = 0.119$ .
- At low dopings from  $p = 0.052$  to  $p = 0.082$  the  $n = 4$  line is augmented by intra unit cell order, spontaneous magnetic fields, and new nematic order. At higher dopings similar signals are seen on the  $n = 2$  line.
- (a) Haug, 2010.<sup>30</sup> Neutron scattering. The temperature reported here marks onset of anisotropy in a neutron scattering triple-axis experiment. This is a sign of nematic order, and is called an electronic liquid crystal.
  - (b) Baledent, 2011.<sup>5</sup> Polarized neutron scattering showing the onset of intra unit cell order, i.e. time reversal symmetry breaking while retaining lattice translational symmetry. The lowest doping data point, at  $p = 0.08$ ,  $T = 170$  K, lies near the  $n = 4$  line (about 13 K higher, within the published error bars of  $\pm 30$  K).
  - (c) Sonier, 2001.<sup>80</sup> Muon spin relaxation. This is the extinction temperature of a signal that indicates the presence of small spontaneous magnetic fields. Two data points. The first lies on the  $n = 4$  line. We omit the second data point, which lies about 35 K below the  $n = 4$  line, well outside the experimental error bars of  $\pm 10$  K, and close to the three dimensional charge density waves<sup>47</sup>.
5. Other Data Sets:
- (a) Arpaia, 2018.<sup>3</sup> Thin film on an MgO substrate. Resistivity. The temperature reported here marks a transition to quadratic at higher temperatures. We omit this data from the linear regressions because it clearly has two parts, one at lower doping which decreases very steeply until it hits the superconducting doping, and a second part which follows the superconducting dome.
  - (b) Arpaia, 2018.<sup>3</sup> Thin film on an SrTiO<sub>3</sub> substrate. Resistivity. The temperature reported here marks a transition to quadratic at higher temperatures.
6. Superconducting  $T_c$ , Neel temperature, and charge density waves:
- (a) Coneri, 2010.<sup>12</sup> Neel temperature measured with muon spin rotation.

- (b) Coneri, 2010.<sup>12</sup>  $T_c$  measured with muon spin rotation.
- (c) Liang, 2006.<sup>51</sup>  $T_c$ .
- (d) Laliberte, 2018.<sup>47</sup> Sound velocity measurements of 3-D charge density wave order. We omit the  $T = 0$  data points at either side of the dome.

#### 7. Omitted Data Sets:

- (a) Hinkov, 2008.<sup>32</sup> Neutron scattering. Polarized neutron scattering showing the onset of intra unit cell order, i.e. time reversal symmetry breaking while retaining lattice translational symmetry. We omit this data point because it seems to have been revised from  $T = 150$  K to  $T = 170$  K in Ref.<sup>5</sup> by the same authors..
- (b) Cyr-Choiniere, 2018 and Daou, 2010.<sup>16,20</sup> Nernst effect. The temperature reported here marks a break from the linear signal seen at higher temperatures. In<sup>20</sup> it is shown that this temperature is the point where anisotropy in the Nernst coefficient is extinguished, at  $p = 0.12, 0.13, 0.15, 0.18$ . The authors argue that this anisotropy is caused by rotational symmetry breaking in the copper oxide planes as opposed to the oxygen chains. Ref.<sup>17</sup> by the same authors, five years later, re-evaluates the data, and says that the Nernst anisotropy seen in Ref.<sup>20</sup> "is more likely to be caused by CDW modulations" instead of the pseudogap. In other words, although they saw the beginning of a slight rise in the Nernst anisotropy at the pseudogap temperature, the real rise doesn't occur until near the lower temperatures where CDW order is observed using X-ray diffraction. Ref.<sup>17</sup> is an effort to sort out where the new nematicity begins. We omit this data set

(but not Ref.<sup>17</sup>) because it was later revised and reinterpreted by the same authors. We also note that the data shows a scatter (compared to its linear regression) of 15 to 20 K, which is above our cutoff for the  $n = 2$  line. This data set cuts across the  $n = 1$  and  $n = 2$  lines and is rather flat.

- (c) Goto, 1996.<sup>27</sup> Nuclear magnetic resonance. The temperature reported here marks a peak in the signal. This data set is very flat and cuts through the  $n = 2$  and  $n = 3$  lines. It roughly coincides with X-ray scattering data on short-range charge density wave order from Ref.<sup>7</sup>.
- (d) Cooper, 1996.<sup>13</sup> Several pseudogap temperature data sets are reported in Figure 30. This data is omitted because we don't understand where it came from and therefore can not verify whether it meets our selection criteria, and also because it seems that the thermoelectric power data in Figure 30 (which runs up to 600 K) was derived from data in Figure 28b, which has a temperature cutoff of 300 K.

#### Acknowledgments

We gratefully acknowledge stimulating discussions with K. S. Kim, J. Zaanen, A. Ho, S. Hayden, M. Surlangi, K. Schalm, V. Cheianov, T. Ziman, I. Vishik, J. Saunders, L. Levitin, J. Koelzer, P. Hasnip, M. Ma, P. Abbamonte, A. Kim, P. Coleman, S. Hayden, and especially A. Petrovic. We thank the Instituut Lorentz in Leiden for hospitality, and the Hubbard Consortium for facilitating discussions. We acknowledge support from EPSRC grant EP/M011038/1.

---

\* Electronic address: vincent@sacksteder.com

<sup>1</sup> H Alloul, F Rullier-Albenque, B Vignolle, D Colson, and A Forget. Superconducting fluctuations, pseudogap and phase diagram in cuprates. *EPL (Europhysics Letters)*, 91(3):37005, 2010.

<sup>2</sup> Yoichi Ando, Seiki Komiya, Kouji Segawa, S. Ono, and Y. Kurita. Electronic phase diagram of high- $T_c$  cuprate superconductors from a mapping of the in-plane resistivity curvature. *Phys. Rev. Lett.*, 93:267001, Dec 2004.

<sup>3</sup> Riccardo Arpaia, Eric Andersson, Edoardo Tralbaldo, Thilo Bauch, and Florian Lombardi. Probing the phase diagram of cuprates with  $\text{yba}_2\text{cu}_3\text{o}_{7-\delta}$  thin films and nanowires. *Phys. Rev. Materials*, 2:024804, Feb 2018.

<sup>4</sup> V. Balédent, B. Fauqué, Y. Sidis, N. B. Christensen, S. Pailhès, K. Conder, E. Pomjakushina, J. Mesot, and P. Bourges. Two-dimensional orbital-like magnetic order in the high-temperature  $\text{la}_{2-x}\text{sr}_x\text{cuo}_4$  superconductor.

*Phys. Rev. Lett.*, 105:027004, Jul 2010.

<sup>5</sup> V. Balédent, D. Haug, Y. Sidis, V. Hinkov, C. T. Lin, and P. Bourges. Evidence for competing magnetic instabilities in underdoped  $\text{yba}_2\text{cu}_3\text{o}_{6+x}$ . *Phys. Rev. B*, 83:104504, Mar 2011.

<sup>6</sup> B Batlogg, H. Y. Hwang, H Takagi, H. L. Kao, J Kwo, and R. J. Cava. Charge dynamics in  $(\text{la}, \text{sr})_2 \text{cuo}_4$ : from underdoping to overdoping. *Journal of Low Temperature Physics*, 95(1-2):23–31, 1994.

<sup>7</sup> S. Blanco-Canosa, A. Frano, E. Schierle, J. Porras, T. Loew, M. Minola, M. Bluschke, E. Weschke, B. Keimer, and M. Le Tacon. Resonant x-ray scattering study of charge-density wave correlations in  $\text{yba}_2\text{cu}_3\text{o}_{6+x}$ . *Phys. Rev. B*, 90:054513, Aug 2014.

<sup>8</sup> G. S. Boebinger, Yoichi Ando, A. Passner, T. Kimura, M. Okuya, J. Shimoyama, K. Kishio, K. Tamasaku, N. Ichikawa, and S. Uchida. Insulator-to-metal crossover

- in the normal state of  $\text{La}_{2-x}\text{Sr}_x\text{CuO}_4$  near optimum doping. *Phys. Rev. Lett.*, 77:5417–5420, Dec 1996.
- 9 I Božović, X He, J Wu, and A T Bollinger. Dependence of the critical temperature in overdoped copper oxides on superfluid density. *Nature*, 536(7616):309, 2016.
  - 10 Utpal Chatterjee, Dingfei Ai, Junjing Zhao, Stephan Rosenkranz, Adam Kaminski, Helene Raffy, Zhizhong Li, Kazuo Kadowaki, Mohit Randeria, Michael R Norman, and J C Campuzano. Electronic phase diagram of high-temperature copper oxide superconductors. *Proceedings of the National Academy of Sciences*, 108(23):9346–9349, 2011.
  - 11 C. Collignon, S. Badoux, S. A. A. Afshar, B. Michon, F. Laliberté, O. Cyr-Choinière, J.-S. Zhou, S. Licciardello, S. Wiedmann, N. Doiron-Leyraud, and Louis Taillefer. Fermi-surface transformation across the pseudogap critical point of the cuprate superconductor  $\text{La}_{1.6-x}\text{Nd}_{0.4}\text{Sr}_x\text{CuO}_4$ . *Phys. Rev. B*, 95:224517, Jun 2017.
  - 12 F. Coneri, S. Sanna, K. Zheng, J. Lord, and R. De Renzi. Magnetic states of lightly hole-doped cuprates in the clean limit as seen via zero-field muon spin spectroscopy. *Phys. Rev. B*, 81:104507, Mar 2010.
  - 13 J R Cooper and J W Loram. Some correlations between the thermodynamic and transport properties of high  $t_c$  oxides in the normal state. *Journal de Physique I*, 6(12):2237–2263, 1996.
  - 14 JR Cooper, JW Loram, Ivan Kokanović, JG Storey, and JL Tallon. Pseudogap in  $\text{YBa}_2\text{Cu}_3\text{O}_{6+\delta}$  is not bounded by a line of phase transitions: thermodynamic evidence. *Physical Review B*, 89(20):201104, 2014.
  - 15 R A Cooper, Y Wang, B Vignolle, O J Lipscombe, S M Hayden, Y Tanabe, T Adachi, Y Koike, M Nohara, H Takagi, C Proust, and N E Hussey. Anomalous criticality in the electrical resistivity of  $\text{La}_{2-x}\text{Sr}_x\text{CuO}_4$ . *Science*, 323(5914):603–607, 2009.
  - 16 O. Cyr-Choinière, R. Daou, F. Laliberté, C. Collignon, S. Badoux, D. LeBoeuf, J. Chang, B. J. Ramshaw, D. A. Bonn, W. N. Hardy, R. Liang, J.-Q. Yan, J.-G. Cheng, J.-S. Zhou, J. B. Goodenough, S. Pyon, T. Takayama, H. Takagi, N. Doiron-Leyraud, and Louis Taillefer. Pseudogap temperature  $T^*$  of cuprate superconductors from the nernst effect. *Phys. Rev. B*, 97:064502, Feb 2018.
  - 17 O. Cyr-Choinière, G. Grissonnanche, S. Badoux, J. Day, D. A. Bonn, W. N. Hardy, R. Liang, N. Doiron-Leyraud, and Louis Taillefer. Two types of nematicity in the phase diagram of the cuprate superconductor  $\text{YBa}_2\text{Cu}_3\text{O}_y$ . *Phys. Rev. B*, 92:224502, Dec 2015.
  - 18 Olivier Cyr-Choiniere, R Daou, Francis Laliberté, David LeBoeuf, Nicolas Doiron-Leyraud, J Chang, J-Q Yan, J-G Cheng, J-S Zhou, J B Goodenough, S Pyon, T Takayama, H Takagi, Y Tanaka, and L Taillefer. Enhancement of the nernst effect by stripe order in a high- $t_c$  superconductor. *Nature*, 458(7239):743, 2009.
  - 19 Pengcheng Dai, Herbert A Mook, Stephen M Hayden, Gabriel Aeppli, Toby G Perring, Rodney Dale Hunt, and F Doğan. The magnetic excitation spectrum and thermodynamics of high- $t_c$  superconductors. *Science*, 284(5418):1344–1347, 1999.
  - 20 R Daou, J Chang, David LeBoeuf, Olivier Cyr-Choiniere, Francis Laliberté, Nicolas Doiron-Leyraud, B J Ramshaw, Ruixing Liang, D A Bonn, W N Hardy, and L Taillefer. Broken rotational symmetry in the pseudogap phase of a high- $t_c$  superconductor. *Nature*, 463(7280):519, 2010.
  - 21 Nicolas Doiron-Leyraud, P Auban-Senzier, S René de Cotret, A Sedeki, C Bourbonnais, D Jerome, K Bechgaard, and Louis Taillefer. Correlation between linear resistivity and  $t_c$  in organic and pnictide superconductors. *arXiv preprint arXiv:0905.0964*, 2009.
  - 22 J Dominec. Ultrasonic and related experiments in high- $t_c$  superconductors. *Superconductor Science and Technology*, 6(3):153, 1993.
  - 23 B. Fauqué, Y. Sidis, V. Hinkov, S. Pailhès, C. T. Lin, X. Chaud, and P. Bourges. Magnetic order in the pseudogap phase of high- $T_c$  superconductors. *Phys. Rev. Lett.*, 96:197001, May 2006.
  - 24 Eduardo Fradkin, Steven A. Kivelson, and John M. Tranquada. Colloquium: Theory of intertwined orders in high temperature superconductors. *Rev. Mod. Phys.*, 87:457–482, May 2015.
  - 25 T. Fujii, T. Matsushima, T. Maruoka, and A. Asamitsu. Effect of stripe order strength for the nernst effect in  $\text{La}_{2-x}\text{Sr}_x\text{CuO}_4$  single crystals. *Physica C: Superconductivity and its Applications*, 470:S21 – S22, 2010. Proceedings of the 9th International Conference on Materials and Mechanisms of Superconductivity.
  - 26 Paula Giraldo-Gallo, JA Galvis, Z Stegen, KA Modic, FF Balakirev, JB Betts, X Lian, C Moir, SC Riggs, J Wu, A T Bollinger, X He, I Bozovic, B J Ramshaw, R D McDonald, G S Boebinger, and A Shekhter. Scale-invariant magnetoresistance in a cuprate superconductor. *Science*, 361(6401):479–481, 2018.
  - 27 Atsushi Goto, Hiroshi Yasuoka, and Yutaka Ueda. Carrier concentration dependence of the spin pseudo-gap behaviors in  $\text{YBa}_2\text{Cu}_3\text{O}_y$ . *Journal of the Physical Society of Japan*, 65(9):3043–3048, 1996.
  - 28 M. Hashimoto, T. Yoshida, K. Tanaka, A. Fujimori, M. Okusawa, S. Wakimoto, K. Yamada, T. Kakeshita, H. Eisaki, and S. Uchida. Distinct doping dependences of the pseudogap and superconducting gap of  $\text{La}_{2-x}\text{Sr}_x\text{CuO}_4$  cuprate superconductors. *Phys. Rev. B*, 75:140503, Apr 2007.
  - 29 M. Hashimoto, T. Yoshida, K. Tanaka, A. Fujimori, M. Okusawa, S. Wakimoto, K. Yamada, T. Kakeshita, H. Eisaki, and S. Uchida. Crossover from coherent quasiparticles to incoherent hole carriers in underdoped cuprates. *Phys. Rev. B*, 79:140502, Apr 2009.
  - 30 Daniel Haug, Vladimir Hinkov, Yvan Sidis, Philippe Bourges, Niels Bech Christensen, Alexandre Ivanov, Thomas Keller, CT Lin, and B Keimer. Neutron scattering study of the magnetic phase diagram of underdoped  $\text{YBa}_2\text{Cu}_3\text{O}_{6+x}$ . *New Journal of Physics*, 12(10):105006, 2010.
  - 31 Ian M Hayes, Ross D McDonald, Nicholas P Breznay, Toni Helm, Philip J W Moll, Mark Wartenbe, Arkady Shekhter, and James G Analytis. Scaling between magnetic field and temperature in the high-temperature superconductor  $\text{BaFe}_2(\text{As}_{1-x}\text{P}_x)_2$ . *Nature Physics*, 12(10):916, 2016.
  - 32 V Hinkov, D Haug, B Fauqué, P Bourges, Y Sidis, A Ivanov, Christian Bernhard, CT Lin, and B Keimer. Electronic liquid crystal state in the high-temperature superconductor  $\text{YBa}_2\text{Cu}_3\text{O}_6$ . *Science*, 319(5863):597–600, 2008.
  - 33 NE Hussey, RA Cooper, Xiaofeng Xu, Y Wang, I Mouzopoulou, B Vignolle, and C Proust. Dichotomy in the  $t$ -linear resistivity in hole-doped cuprates. *Philosophical Transactions of the Royal Society of London A: Mathematical, Physical and Engineering Sciences*,

- 369(1941):1626–1639, 2011.
- <sup>34</sup> H. Y. Hwang, B. Batlogg, H. Takagi, H. L. Kao, J. Kwo, R. J. Cava, J. J. Krajewski, and W. F. Peck. Scaling of the temperature dependent hall effect in  $\text{La}_{2-x}\text{Sr}_x\text{CuO}_4$ . *Phys. Rev. Lett.*, 72:2636–2639, Apr 1994.
- <sup>35</sup> N. Ichikawa, S. Uchida, J. M. Tranquada, T. Niemöller, P. M. Gehring, S.-H. Lee, and J. R. Schneider. Local magnetic order vs superconductivity in a layered cuprate. *Phys. Rev. Lett.*, 85:1738–1741, Aug 2000.
- <sup>36</sup> A. Ino, T. Mizokawa, K. Kobayashi, A. Fujimori, T. Sasagawa, T. Kimura, K. Kishio, K. Tamasaku, H. Eisaki, and S. Uchida. Doping dependent density of states and pseudogap behavior in  $\text{La}_{2-x}\text{Sr}_x\text{CuO}_4$ . *Phys. Rev. Lett.*, 81:2124–2127, Sep 1998.
- <sup>37</sup> Y. Itoh, T. Machi, N. Koshizuka, M. Murakami, H. Yamagata, and M. Matsumura. Pseudo-spin-gap and slow spin fluctuation in  $\text{La}_{2-x}\text{Sr}_x\text{CuO}_4$  ( $x = 0.13$  and  $0.18$ ) via  $^{63}\text{Cu}$  and  $^{139}\text{La}$  nuclear quadrupole resonance. *Phys. Rev. B*, 69:184503, May 2004.
- <sup>38</sup> David C. Johnston. Magnetic susceptibility scaling in  $\text{La}_{2-x}\text{Sr}_x\text{CuO}_{4-y}$ . *Phys. Rev. Lett.*, 62:957–960, Feb 1989.
- <sup>39</sup> V. V. Kabanov, J. Demsar, B. Podobnik, and D. Mihailovic. Quasiparticle relaxation dynamics in superconductors with different gap structures: Theory and experiments on  $\text{YBa}_2\text{Cu}_3\text{O}_{7-\delta}$ . *Phys. Rev. B*, 59:1497–1506, Jan 1999.
- <sup>40</sup> Aharon Kapitulnik, Jing Xia, Elizabeth Schemm, and Alexander Palevski. Polar kerr effect as probe for time-reversal symmetry breaking in unconventional superconductors. *New Journal of Physics*, 11(5):055060, 2009.
- <sup>41</sup> B. Keimer, A. Aharony, A. Auerbach, R. J. Birgeneau, A. Cassanho, Y. Endoh, R. W. Erwin, M. A. Kastner, and G. Shirane. Néel transition and sublattice magnetization of pure and doped  $\text{La}_2\text{CuO}_4$ . *Phys. Rev. B*, 45:7430–7435, Apr 1992.
- <sup>42</sup> B. Keimer, N. Belk, R. J. Birgeneau, A. Cassanho, C. Y. Chen, M. Greven, M. A. Kastner, A. Aharony, Y. Endoh, R. W. Erwin, and G. Shirane. Magnetic excitations in pure, lightly doped, and weakly metallic  $\text{La}_2\text{CuO}_4$ . *Phys. Rev. B*, 46:14034–14053, Dec 1992.
- <sup>43</sup> B Keimer, S A Kivelson, M R Norman, S Uchida, and J Zaanen. From quantum matter to high-temperature superconductivity in copper oxides. *Nature*, 518(7538):179, 2015.
- <sup>44</sup> J. S. Kim, B. H. Kim, D. C. Kim, and Y. W. Park. Two pseudogap behavior in  $\text{La}_{2-x}\text{Sr}_x\text{CuO}_4$ : Thermoelectric power at high temperature. *Journal of superconductivity*, 17(1):151–157, 2004.
- <sup>45</sup> Rohit Kumar, Surjeet Singh, and Sunil Nair. High temperature linear magnetoresistance and scaling behavior in the  $\text{Ba}(\text{Fe}_{1-x}\text{Co}_x)_2\text{As}_2$  series. *arXiv preprint arXiv:1801.03768*, 2018.
- <sup>46</sup> F Laliberté, W Tabis, S Badoux, B Vignolle, D Destraz, N Momono, T Kurosawa, K Yamada, H Takagi, N Doiron-Leyraud, C Proust, and L Taillefer. Origin of the metal-to-insulator crossover in cuprate superconductors. *arXiv preprint arXiv:1606.04491*, 2016.
- <sup>47</sup> Francis Laliberté, Mehdi Frachet, Siham Benhabib, Benjamin Borgnic, Toshinao Loew, Juan Porras, Mathieu Tacon, Bernhard Keimer, Steffen Wiedmann, Cyril Proust, and David LeBoeuf. High field charge order across the phase diagram of  $\text{YBa}_2\text{Cu}_3\text{O}_y$ . *npj Quantum Materials*, 3(1):11, 2018.
- <sup>48</sup> A N Lavrov. Low temperature order-disorder phenomena in  $\text{YBa}_2\text{Cu}_3\text{O}_{7-x}$ : an electrical resistivity study. *Physics Letters A*, 168(1):71–74, 1992.
- <sup>49</sup> David LeBoeuf, Nicolas Doiron-Leyraud, B. Vignolle, Mike Sutherland, B. J. Ramshaw, J. Levallois, R. Daou, Francis Laliberté, Olivier Cyr-Choinière, Johan Chang, Y. J. Jo, L. Balicas, Ruixing Liang, D. A. Bonn, W. N. Hardy, Cyril Proust, and Louis Taillefer. Lifshitz critical point in the cuprate superconductor  $\text{YBa}_2\text{Cu}_3\text{O}_y$  from high-field hall effect measurements. *Phys. Rev. B*, 83:054506, Feb 2011.
- <sup>50</sup> B Leridon, P Monod, D Colson, and A Forget. Thermodynamic signature of a phase transition in the pseudogap phase of  $\text{YBa}_2\text{Cu}_3\text{O}_x$  high- $T_c$  superconductor. *EPL (Europhysics Letters)*, 87(1):17011, 2009.
- <sup>51</sup> Ruixing Liang, D. A. Bonn, and W. N. Hardy. Evaluation of  $\text{CuO}_2$  plane hole doping in  $\text{YBa}_2\text{Cu}_3\text{O}_{6+x}$  single crystals. *Phys. Rev. B*, 73:180505, May 2006.
- <sup>52</sup> Y. Lubashevsky, LiDong Pan, T. Kirzhner, G. Koren, and N. P. Armitage. Optical birefringence and dichroism of cuprate superconductors in the thz regime. *Phys. Rev. Lett.*, 112:147001, Apr 2014.
- <sup>53</sup> M. Majoros, C. Panagopoulos, T. Nishizaki, and H. Iwasaki. Thermomagnetic hysteretic properties resembling superconductivity in the normal state of  $\text{La}_{1.85}\text{Sr}_{0.15}\text{CuO}_4$ . *Phys. Rev. B*, 72:024528, Jul 2005.
- <sup>54</sup> L Mangin-Thro, Y Sidis, A Wildes, and P Bourges. Intra-unit-cell magnetic correlations near optimal doping in  $\text{YBa}_2\text{Cu}_3\text{O}_{6.85}$ . *Nature communications*, 6:7705, 2015.
- <sup>55</sup> Lucile Mangin-Thro, Yuan Li, Yvan Sidis, and Philippe Bourges.  $a - b$  anisotropy of the intra-unit-cell magnetic order in  $\text{YBa}_2\text{Cu}_3\text{O}_{6.6}$ . *Phys. Rev. Lett.*, 118:097003, Mar 2017.
- <sup>56</sup> M. Matsuda, M. Fujita, K. Yamada, R. J. Birgeneau, Y. Endoh, and G. Shirane. Electronic phase separation in lightly doped  $\text{La}_{2-x}\text{Sr}_x\text{CuO}_4$ . *Phys. Rev. B*, 65:134515, Mar 2002.
- <sup>57</sup> Toshiaki Matsuzaki, Naoki Momono, Migaku Oda, and Masayuki Ido. Electronic specific heat of  $\text{La}_{2-x}\text{Sr}_x\text{CuO}_4$ : Pseudogap formation and reduction of the superconducting condensation energy. *Journal of the Physical Society of Japan*, 73(8):2232–2238, 2004.
- <sup>58</sup> C. E. Matt, C. G. Fatuzzo, Y. Sassa, M. Månsson, S. Fatale, V. Bitetta, X. Shi, S. Pailhès, M. H. Berntsen, T. Kurosawa, M. Oda, N. Momono, O. J. Lipscombe, S. M. Hayden, J.-Q. Yan, J.-S. Zhou, J. B. Goodenough, S. Pyon, T. Takayama, H. Takagi, L. Patthey, A. Bendounan, E. Razzoli, M. Shi, N. C. Plumb, M. Radovic, M. Grioni, J. Mesot, O. Tjernberg, and J. Chang. Electron scattering, charge order, and pseudogap physics in  $\text{La}_{1.6-x}\text{Nd}_{0.4}\text{Sr}_x\text{CuO}_4$ : An angle-resolved photoemission spectroscopy study. *Phys. Rev. B*, 92:134524, Oct 2015.
- <sup>59</sup> G. P. Mikitik and Yu. V. Sharlai. Manifestation of berry's phase in metal physics. *Phys. Rev. Lett.*, 82:2147–2150, Mar 1999.
- <sup>60</sup> N Momono and M Ido. Evidence for nodes in the superconducting gap of  $\text{La}_{2-x}\text{Sr}_x\text{CuO}_4$ .  $t^2$  dependence of electronic specific heat and impurity effects. *Physica C: Superconductivity*, 264(3-4):311–318, 1996.
- <sup>61</sup> N Momono, M Ido, T Nakano, M Oda, Y Okajima, and K Yamaya. Low-temperature electronic specific heat of  $\text{La}_{2-x}\text{Sr}_x\text{CuO}_4$  and  $\text{La}_{2-x}\text{Sr}_x\text{Cu}_{1-y}\text{Zn}_y\text{O}_4$ . evidence for ad wave superconductor. *Physica C: Superconductivity*, 233(3-4):395–401, 1994.
- <sup>62</sup> H. A. Mook, Y. Sidis, B. Fauqué, V. Balédent, and

- P. Bourges. Observation of magnetic order in a superconducting  $\text{YBa}_2\text{Cu}_3\text{O}_{6.6}$  single crystal using polarized neutron scattering. *Phys. Rev. B*, 78:020506, Jul 2008.
- <sup>63</sup> Peter Nagel, Volker Pasler, Christoph Meingast, Alexandre I. Rykov, and Setsuko Tajima. Anomalously large oxygen-ordering contribution to the thermal expansion of untwinned  $\text{YBa}_2\text{Cu}_3\text{O}_{6.95}$  single crystals: A glasslike transition near room temperature. *Phys. Rev. Lett.*, 85:2376–2379, Sep 2000.
- <sup>64</sup> T. Nakano, M. Oda, C. Manabe, N. Momono, Y. Miura, and M. Ido. Magnetic properties and electronic conduction of superconducting  $\text{La}_{2-x}\text{Sr}_x\text{CuO}_4$ . *Phys. Rev. B*, 49:16000–16008, Jun 1994.
- <sup>65</sup> Tohru Nakano, Naoki Momono, Migaku Oda, and Masayuki Ido. Correlation between the doping dependences of superconducting gap magnitude  $2\delta_0$  and pseudogap temperature  $t^*$  in high- $T_c$  cuprates. *Journal of the Physical Society of Japan*, 67(8):2622–2625, 1998.
- <sup>66</sup> Ch. Niedermayer, C. Bernhard, T. Blasius, A. Golnik, A. Moodenbaugh, and J. I. Budnick. Common phase diagram for antiferromagnetism in  $\text{La}_{2-x}\text{Sr}_x\text{CuO}_4$  and  $\text{Y}_{1-x}\text{Ca}_x\text{Ba}_2\text{Cu}_3\text{O}_6$  as seen by muon spin rotation. *Phys. Rev. Lett.*, 80:3843–3846, Apr 1998.
- <sup>67</sup> Takashi Nishikawa, Jun Takeda, and Masatoshi Sato. Transport anomalies of high- $T_c$  oxides above room temperature. *Journal of the Physical Society of Japan*, 63(4):1441–1448, 1994.
- <sup>68</sup> M R Norman, D Pines, and C Kallin. The pseudogap: friend or foe of high  $T_c$ ? *Advances in Physics*, 54(8):715–733, 2005.
- <sup>69</sup> M Oda, H Matsuki, and M Ido. Common features of magnetic and superconducting properties in y-doped  $\text{Bi}_2(\text{Sr}, \text{Ca})_3\text{Cu}_2\text{O}_8$  and ba (sr)-doped  $\text{La}_2\text{CuO}_4$ . *Solid State Communications*, 74(12):1321–1326, 1990.
- <sup>70</sup> M Oda, T Nakano, Y Kamada, and M Ido. Electronic states of doped holes and magnetic properties in  $\text{La}_{2-x}\text{M}_x\text{CuO}_4$  (m= sr, ba). *Physica C: Superconductivity*, 183(4-6):234–240, 1991.
- <sup>71</sup> M Oda, T Ohguro, H Matsuki, N Yamada, and M Ido. Magnetism and superconductivity in doped  $\text{La}_2\text{CuO}_4$ . *Physical Review B*, 41(4):2605, 1990.
- <sup>72</sup> Shigeaki Ohsugi, Yoshio Kitaoka, Kenji Ishida, and Kunisuke Asayama. Cu nqr study of the spin dynamics in high- $T_c$  superconductor  $\text{La}_{2-x}\text{Sr}_x\text{CuO}_4$ . *Journal of the Physical Society of Japan*, 60(7):2351–2360, 1991.
- <sup>73</sup> C. Panagopoulos, M. Majoros, T. Nishizaki, and H. Iwasaki. Weak magnetic order in the normal state of the high- $T_c$  superconductor  $\text{La}_{2-x}\text{Sr}_x\text{CuO}_4$ . *Phys. Rev. Lett.*, 96:047002, Feb 2006.
- <sup>74</sup> C. Panagopoulos, M. Majoros, and A. P. Petrović. Thermal hysteresis in the normal-state magnetization of  $\text{La}_{2-x}\text{Sr}_x\text{CuO}_4$ . *Phys. Rev. B*, 69:144508, Apr 2004.
- <sup>75</sup> Vincent Sacksteder. Fermion loops, linear magnetoresistance, linear in temperature resistance, and superconductivity. *arXiv preprint arXiv:1801.02663*, 2018.
- <sup>76</sup> Y Sato, S Kasahara, H Murayama, Y Kasahara, E-G Moon, T Nishizaki, T Loew, J Porras, B Keimer, T Shibauchi, and T Matsuda. Thermodynamic evidence for a nematic phase transition at the onset of the pseudogap in  $\text{YBa}_2\text{Cu}_3\text{O}_y$ . *Nature Physics*, 13(11):1074, 2017.
- <sup>77</sup> Kouji Segawa and Yoichi Ando. Intrinsic hall response of the  $\text{CuO}_2$  planes in a chain-plane composite system of  $\text{YBa}_2\text{Cu}_3\text{O}_y$ . *Phys. Rev. B*, 69:104521, Mar 2004.
- <sup>78</sup> Arkady Shekhter, B J Ramshaw, Ruixing Liang, W N Hardy, D A Bonn, Fedor F Balakirev, Ross D McDonald, Jon B Betts, Scott C Riggs, and Albert Migliori. Bounding the pseudogap with a line of phase transitions in  $\text{YBa}_2\text{Cu}_3\text{O}_{6+\delta}$ . *Nature*, 498(7452):75, 2013.
- <sup>79</sup> Yvan Sidis, Benoit Fauqué, Vivek Aji, and Philippe Bourges. Search for the existence of circulating currents in high- $T_c$  superconductors using the polarized neutron scattering technique. *Physica B: Condensed Matter*, 397(1-2):1–6, 2007.
- <sup>80</sup> J E Sonier, J H Brewer, R F Kiefl, R I Miller, G D Morris, C E Stronach, J S Gardner, S R Dunsiger, D A Bonn, W N Hardy, R Liang, and R H Heffner. Anomalous weak magnetism in superconducting  $\text{YBa}_2\text{Cu}_3\text{O}_{6+x}$ . *Science*, 292(5522):1692–1695, 2001.
- <sup>81</sup> Jeff E Sonier. Comment on” discovery of slow magnetic fluctuations and critical slowing down in the pseudogap phase of  $\text{YBa}_2\text{Cu}_3\text{O}_{6-y}$ ”. *arXiv preprint arXiv:1706.03023*, 2017.
- <sup>82</sup> T. Startseva, T. Timusk, A. V. Puchkov, D. N. Basov, H. A. Mook, M. Okuya, T. Kimura, and K. Kishio. Temperature evolution of the pseudogap state in the infrared response of underdoped  $\text{La}_{2-x}\text{Sr}_x\text{CuO}_4$ . *Phys. Rev. B*, 59:7184–7190, Mar 1999.
- <sup>83</sup> H. Takagi, R. J. Cava, M. Marezio, B. Batlogg, J. J. Krajewski, W. F. Peck, P. Bordet, and D. E. Cox. Disappearance of superconductivity in overdoped  $\text{La}_{2-x}\text{Sr}_x\text{CuO}_4$  at a structural phase boundary. *Phys. Rev. Lett.*, 68:3777–3780, Jun 1992.
- <sup>84</sup> T Takemura, T Kitajima, T Sugaya, and I Terasaki. Scaling behaviour of the in-plane thermopower in  $\text{Bi}_2\text{Sr}_r\text{Cu}_2\text{O}_8$  (r= ca, y, pr, dy and er). *Journal of Physics: Condensed Matter*, 12(28):6199, 2000.
- <sup>85</sup> J L Tallon, J W Loram, G V M Williams, J R Cooper, I R Fisher, J D Johnson, M P Staines, and C Bernhard. Critical doping in overdoped high- $T_c$  superconductors: a quantum critical point? *Physica Status Solidi B*, 215:531–540, 1999.
- <sup>86</sup> Y. J. Uemura, G. M. Luke, B. J. Sternlieb, J. H. Brewer, J. F. Carolan, W. N. Hardy, R. Kadono, J. R. Kempton, R. F. Kiefl, S. R. Kreitzman, P. Mulhern, T. M. Rise-man, D. Ll. Williams, B. X. Yang, S. Uchida, H. Takagi, J. Gopalakrishnan, A. W. Sleight, M. A. Subramanian, C. L. Chien, M. Z. Cieplak, Gang Xiao, V. Y. Lee, B. W. Statt, C. E. Stronach, W. J. Kossler, and X. H. Yu. Universal correlations between  $T_c$  and  $\frac{n_s}{m^*}$  (carrier density over effective mass) in high- $T_c$  cuprate superconductors. *Phys. Rev. Lett.*, 62:2317–2320, May 1989.
- <sup>87</sup> I M Vishik. Photoemission perspective on pseudogap, superconducting fluctuations, and charge order in cuprates: a review of recent progress. *Reports on Progress in Physics*, 81(6):062501, 2018.
- <sup>88</sup> Yayu Wang, Lu Li, and N. P. Ong. Nernst effect in high- $T_c$  superconductors. *Phys. Rev. B*, 73:024510, Jan 2006.
- <sup>89</sup> Yayu Wang, Z. A. Xu, T. Kakeshita, S. Uchida, S. Ono, Yoichi Ando, and N. P. Ong. Onset of the vortexlike nernst signal above  $T_c$  in  $\text{La}_{2-x}\text{Sr}_x\text{CuO}_4$  and  $\text{Bi}_2\text{Sr}_{2-y}\text{La}_y\text{CuO}_6$ . *Phys. Rev. B*, 64:224519, Nov 2001.
- <sup>90</sup> Yue Wang and Jun Zhang. Revisiting the electronic phase diagram of  $\text{YBa}_2\text{Cu}_3\text{O}_y$  via temperature derivative of in-plane resistivity. *arXiv preprint arXiv:1711.07402*, 2017.
- <sup>91</sup> J Wu, A T Bollinger, X He, and I Božović. Spontaneous breaking of rotational symmetry in copper oxide superconductors. *Nature*, 547(7664):432, 2017.
- <sup>92</sup> B. Wuyts, V. V. Moshchalkov, and Y. Bruynseraede.

- Resistivity and hall effect of metallic oxygen-deficient  $\text{Yb}_{a_2}\text{Cu}_3\text{O}_x$  films in the normal state. *Phys. Rev. B*, 53:9418–9432, Apr 1996.
- <sup>93</sup> Jing Xia, Elizabeth Schemm, G. Deutscher, S. A. Kivelson, D. A. Bonn, W. N. Hardy, R. Liang, W. Siemons, G. Koster, M. M. Fejer, and A. Kapitulnik. Polar kerr-effect measurements of the high-temperature  $\text{Yb}_{a_2}\text{Cu}_3\text{O}_{6+x}$  superconductor: Evidence for broken symmetry near the pseudogap temperature. *Phys. Rev. Lett.*, 100:127002, Mar 2008.
- <sup>94</sup> Dongwei Xu, Junjie Qi, Jie Liu, Vincent Sacksteder, X. C. Xie, and Hua Jiang. Phase structure of the topological anderson insulator. *Phys. Rev. B*, 85:195140, May 2012.
- <sup>95</sup> Z A Xu, N P Ong, T Kakeshita, H Eisaki, and S Uchida. Charge transport in  $\text{La}_{2-x}\text{Sr}_x\text{CuO}_4$  in the low-density limit ( $0.03 \leq x \leq 0.10$ ). *Physica C: Superconductivity*, 341:1711–1714, 2000.
- <sup>96</sup> Z A Xu, N P Ong, Yayu Wang, T Kakeshita, and S Uchida. Vortex-like excitations and the onset of superconducting phase fluctuation in underdoped  $\text{La}_{2-x}\text{Sr}_x\text{CuO}_4$ . *Nature*, 406(6795):486, 2000.
- <sup>97</sup> K. Yamada, C. H. Lee, K. Kurahashi, J. Wada, S. Wakimoto, S. Ueki, H. Kimura, Y. Endoh, S. Hosoya, G. Shirane, R. J. Birgeneau, M. Greven, M. A. Kastner, and Y. J. Kim. Doping dependence of the spatially modulated dynamical spin correlations and the superconducting-transition temperature in  $\text{La}_{2-x}\text{Sr}_x\text{CuO}_4$ . *Phys. Rev. B*, 57:6165–6172, Mar 1998.
- <sup>98</sup> T. Yoshida, M. Hashimoto, S. Ideta, A. Fujimori, K. Tanaka, N. Mannella, Z. Hussain, Z.-X. Shen, M. Kubota, K. Ono, Seiki Komiya, Yoichi Ando, H. Eisaki, and S. Uchida. Universal versus material-dependent two-gap behaviors of the high- $T_c$  cuprate superconductors: Angle-resolved photoemission study of  $\text{La}_{2-x}\text{Sr}_x\text{CuO}_4$ . *Phys. Rev. Lett.*, 103:037004, Jul 2009.
- <sup>99</sup> R Yoshizaki, N Ishikawa, H Sawada, E Kita, and A Tasaki. Magnetic susceptibility of normal state and superconductivity of  $\text{La}_{2-x}\text{Sr}_x\text{CuO}_4$ . *Physica C: Superconductivity*, 166(5-6):417–422, 1990.
- <sup>100</sup> Jian Zhang, Zhaofeng Ding, Cheng Tan, Kevin Huang, Oscar O Bernal, Pei-Chun Ho, Gerald D Morris, Adrian D Hillier, Pabitra K Biswas, Stephen P Cottrell, Hui Xiang, Xin Yao, Douglas E MacLaughlin, and Lei Shu. Discovery of slow magnetic fluctuations and critical slowing down in the pseudogap phase of  $\text{Yb}_{a_2}\text{Cu}_3\text{O}_y$ . *Science advances*, 4(1):eaao5235, 2018.
- <sup>101</sup> L Zhao, C A Belvin, R Liang, D A Bonn, W N Hardy, N P Armitage, and D Hsieh. A global inversion-symmetry-broken phase inside the pseudogap region of  $\text{Yb}_{a_2}\text{Cu}_3\text{O}_y$ . *Nature Physics*, 13(3):250, 2017.
- <sup>102</sup> These sets are labeled in the appendix as  $n = 3$  set (e) and  $n = 4$  sets (d,e,f,g).
- <sup>103</sup> These sets are labeled in the appendix as Omitted Data Sets (a,p,q).
- <sup>104</sup> These sets are labeled in the appendix as  $n = 4$  sets (d,e,f,g).
- <sup>105</sup> We place the intersection at  $p = 0.26$ ,  $T = 0$  K and align the second pseudogap line to the experimental data point in<sup>42</sup> at  $p = 0$ ,  $T = 515$  K.
- <sup>106</sup> The average value of  $n \times dT/dp$ , which is approximately constant because the pseudogap slope varies as  $dT/dp \propto 1/n$ , is 4000 K, and the standard deviation of this value across the fifteen data sets in the first four pseudogap lines is 800 K.
- <sup>107</sup> These sets are labeled in the appendix as  $n = 2$  sets (e,k,l), and show scatters of  $\pm 30$  K, which is substantially larger than the  $\pm 15$  K shown by the other  $n = 2$  data sets.
- <sup>108</sup> This is labeled in the appendix as Omitted Data Sets (c).
- <sup>109</sup> We align the  $n = 2$  pseudogap line to  $p = 0$ ,  $T = 500$  K and  $p = 0.215$ ,  $T = 0$ .
- <sup>110</sup> We have not included the regression of one of the low temperature (purple) data sets which clearly does not follow a linear trajectory, and instead seems to be composed of two line segments.
- <sup>111</sup> It may be worth noting that at  $p = 0$  the  $n = 1$  line’s temperature  $T = 1000$  K, if converted to area  $A$  via  $\hbar^2 A^{-1}/2m_e = k_B T$ , gives an area  $A = 158 a_0^2$ . This is three times the area of the copper oxide unit cell.
- <sup>112</sup> Judging from authors’ estimates, comparison of data sets to their linear regressions, and comparison between data sets, most data sets show scatters or errors of  $\pm 10$  to  $\pm 20$  Kelvin. A notable exception is<sup>78</sup>, which reports that YBCO’s  $n = 2$  pseudogap line has a width of 3 K. There are also several data sets with exceptionally large scatters of 50 K or more, including three out of four data sets on LSCO’s  $n = 1$  line and also the thermoelectric power data on LSCO’s  $n = 2$  line.<sup>44,64,99</sup> We have not included in our figures three data sets on YBCO’s  $n = 2$  pseudogap line because their scatters are larger than  $15$  K<sup>39,50</sup>, including neutron scattering data revealing intra unit cell order.<sup>5,23,54,55,62,79</sup>